Available online at www.sciencedirect.com

ScienceDirect

Geochimica et Cosmochimica Acta 152 (2015) 1–38

Geochimica et Cosmochimica Acta

www.elsevier.com/locate/gca

High spatial resolution geochemistry and textural characteristics of 'microtektite' glass spherules in proximal Cretaceous–Paleogene sections: Insights into glass alteration patterns and precursor melt lithologies

Joke Belza [a,*], Steven Goderis [a,b], Jan Smit [c], Frank Vanhaecke [b], Kitty Baert [d], Herman Terryn [d], Philippe Claeys [a]

[a] *Department of Analytical Environmental and Geo-Chemistry, Vrije Universiteit Brussel, Pleinlaan 2, BE-1050 Brussels, Belgium*
[b] *Department of Analytical Chemistry, Universiteit Gent, Krijgslaan 281-S12, BE-9000 Ghent, Belgium*
[c] *Department of Sedimentology, Vrije Universiteit Amsterdam, de Boelelaan 1085, 1081HV Amsterdam, Netherlands*
[d] *Department of Electrochemical and Surface Engineering, Vrije Universiteit Brussel, Pleinlaan 2, BE-1050 Brussels, Belgium*

Received 10 March 2014; accepted in revised form 9 December 2014; Available online 17 December 2014

Abstract

Using laser ablation-inductively coupled plasma-mass spectrometry (LA-ICP-MS), we have conducted spatially resolved trace element analysis on fresh, unaltered microtektite glasses linked to the Cretaceous–Paleogene (K–Pg) boundary Chicxulub crater and on their surrounding alteration phases. This unique approach offers the opportunity to study *in situ* and at high spatial resolution both the mixing of different target lithologies and the variation of the major and trace element budget during the alteration process. In addition, two-dimensional element distribution maps reveal important geochemical information beyond the capabilities of single spot laser drilling. Glasses from two localities in opposite quadrants from the source crater were studied. At the Beloc locality (Haiti), the glass population is dominated by the presence of yellow high-Ca glass and black andesitic glass formed by admixture of carbonate/dolomite/anhydrite platform lithologies with crystalline basement. These glasses alter according to the well-established hydration–palagonitization model postulated for mafic volcanic glasses. REEs become progressively leached from the glass to below the detection limit for the applied spot size, while immobile Zr, Hf, Nb, and Ta passively accumulate in the process exhibiting both inter-element ratios and absolute concentrations similar to those for the original glass. In contrast, The Arroyo El Mimbral locality (NE Mexico) is characterized by abundant green glass fragments high in Si, Al and alkalis, and low in Mg, Ca, Fe. Low Si black glass is less abundant though similar in composition to the black glass variety at Beloc. The alteration pattern of high-Si, Al green glass at the Mimbral locality is more complex, including numerous competing reaction processes (ion-exchange, hydration, dissolution, and secondary mineral precipitation) generally controlled by the pH and composition of the surrounding fluid. All green, high-Si, Al glasses are hydrated and variably enriched in Sr, Ba, and Cs, indicating preferred adsorption from seawater during hydration. Despite the onset of ion-exchange reactions, which only seem to have affected the alkalis, the trace element composition of the green high-Si, Al glass is still largely representative of the original melt composition. Refining the geochemical signature of (altered) melt lithologies may advance our current understanding of glass stability in the natural environment and provide insight into the origin and emplacement of ejecta material during crater formation.
© 2014 Elsevier Ltd. All rights reserved.

* Corresponding author.
E-mail address: jbelza@vub.ac.be (J. Belza).

http://dx.doi.org/10.1016/j.gca.2014.12.013
0016-7037/© 2014 Elsevier Ltd. All rights reserved.

1. INTRODUCTION

A large number of studies recognize that impact melt holds key information on important parameters to understand the formation of an impact crater (Hörz, 1982; Shaw and Wasserburg, 1982; Glass et al., 1984; Koeberl, 1986; Schuraytz et al., 1994; Warren et al., 1996; Dressler and Reimold, 2001; Claeys et al., 2003; Kettrup and Deutsch, 2003). Because impact melt essentially represents the molten, quenched state of the precursor target, its chemical and isotopic signatures provide a unique fingerprint that is characteristic of the different target rock compositions (Premo and Izett, 1992). Comparative geochemical studies between melt and precursor target materials provide information on depth of excavation, zones of melting and the relative contributions of different target lithologies and (possible traces of) the meteorite impactor variably admixed within the melt. Such parameters are necessary to gain insight into the basic processes of complex crater formation, refine mathematical models, estimate the amount of energy involved in the impact process, etc. (Melosh, 1989; Kring, 1995; Pierazzo et al., 1997, 1998; Pierazzo and Melosh, 1999; Kettrup et al., 2000; Wünnemann et al., 2008).

In the proximal ejecta deposits located all around the Gulf of Mexico and in the Caribbean area, impact melt from the Chicxulub crater occurs predominantly in the form of mm- sized 'glassy spherules', termed 'microtektites' (Bohor and Betterton, 1993). Microtektites are thought to represent droplets of melt, which travelled ballistically from the point of impact and quenched rapidly during flight (Smit, 1999). This interpretation relies on (1) their aerodynamic shape, (2) the lack of crystals or primary microlites, (3) the presence of vesicles documenting an exsolving gas phase that became trapped in a rapidly solidifying melt, (4) an almost zero gas pressure within these bubbles (Smit, 1999), and (5) their stratigraphic position (see Smit et al., 1992a,b, for detailed overview). Chicxulub spherules commonly occur at the base of reworked impact-induced tsunami-wave and deep water oscillatory-wave deposits triggered by the impact event (Smit et al., 1992a,b; Smit, 1999). They are physically separated from the uppermost platinum group element (PGE)-enriched clay layer that marks the late-stage settlement from a mixed target-projectile-rich impact vapor plume (Fig. 1).

2. GEOLOGICAL BACKGROUND

Relict glass from the 66 Ma Chicxulub crater (Yucatán, Mexico) was first described at the Beloc locality (Southern Peninsula of Haiti) (Maurasse et al., 1979; Izett et al., 1990; Sigurdsson et al., 1991a) and at Arroyo El Mimbral (Northeastern Mexico, Smit et al., 1992a,b) (Fig. 1). The discovery of the microtektites allowed the first isotopic dating of the K–Pg impact event (Izett et al., 1991; Swisher et al., 1992) and the acquisition of geochemical data (Izett et al., 1991; Premo and Izett, 1991, 1992; Koeberl, 1993) hinting towards their provenance (Izett et al., 1990, 1991; Sigurdsson et al., 1991a). The striking similarity (both in terms of geochemistry and age) with the in-crater melt sheet unequivocally tied the K–Pg microtektite spherules to Chicxulub as the source crater (Kring and Boynton, 1991, 1992; Swisher et al., 1992; Blum et al., 1993). Microtektite glasses show a compositional range between two distinct end members: a SiO_2-rich black glass and a CaO-rich (and SO_2-rich) yellow glass (Kring and Boynton, 1991; Sigurdsson et al., 1991a,b). On a diagram of $^{87}Sr/^{86}Sr$ versus $\delta^{18}O$, the glasses fall onto a mixing line defined by Cretaceous marine carbonates/evaporites and the in-crater melt sheet with an andesitic composition (Blum et al., 1993). This is largely consistent with a mixture of the main target lithologies beneath Chicxulub, consisting of an upper sedimentary sequence of marine carbonate platform lithologies (alternating carbonate/dolomite/anhydrite) and a crystalline basement (comprised mostly of gneiss, granite, minor amphibolites) (López-Ramos, 1975; Ward et al., 1995; Kettrup and Deutsch, 2003; Urrutia-Fucugauchi et al., 2004). In the mid-nineties, several additional spherule deposits were discovered at numerous sites along the NE Gulf of Mexico (El Peñon, La Sierrita, Rancho Nuevo, Coxqhui, La Lajilla; Alvarez et al., 1992a,b; Smit and Alvarez, 1991; Smit et al., 1996; see Fig. 1).

Although glassy spherules have been crucial in linking the Chicxulub crater with the proximal K–Pg sections, details on their origin and formation mechanism still remain poorly constrained. This is mostly due to the fact that in most localities, spherules are severely altered. Pristine, unaltered glass is very scarce and only rarely found in the center of a smectite/chlorite alteration shell. To date, true glass has only been reported from Beloc (abundant), Arroyo El Mimbral (scarce) and La Lajilla (very scarce). Consequently, several studies on K–Pg microtektite spherules report geochemical data for the alteration phases (Kettrup et al., 2000; Kettrup and Deutsch, 2003; Schulte et al., 2003), instead of the actual glass phases, to derive information on precursor target lithologies. This may lead to ambiguous interpretations concerning the original composition of the melts. For example, at La Sierrita (Fig. 1), Mg–Fe rich (altered) spherules are thought to originate from a more mafic precursor (Schulte et al., 2003). Also, glassy spherules from Chicxulub are not 'tektites' *sensu stricto*: the term 'microtektite' essentially refers to a formation mechanism in which the melts are formed from the uppermost (~200 m) surficial target lithologies (Koeberl, 1993), which is not in agreement with the K–Pg microtektite glass compositions that indicate a much deeper source (down to 4000 m) (Fig. 2).

3. SAMPLES AND ANALYTICAL METHODS

Novel, present-day techniques offer extraction of *in situ* geochemical information at high spatial resolution (μm-scale). Laser ablation-inductively coupled plasma-mass spectrometry (LA-ICP-MS) is a fast, quasi non-destructive analytical technique that provides multi-element determination of major and trace elements at low limits of detection and high spatial resolution. Based on LA-ICP-MS results, combined with whole rock wet chemistry for the determination of major and trace elements, classical petrographic techniques, including scanning electron microscopy (SEM), electron probe microanalysis (EPMA), and micro-Raman

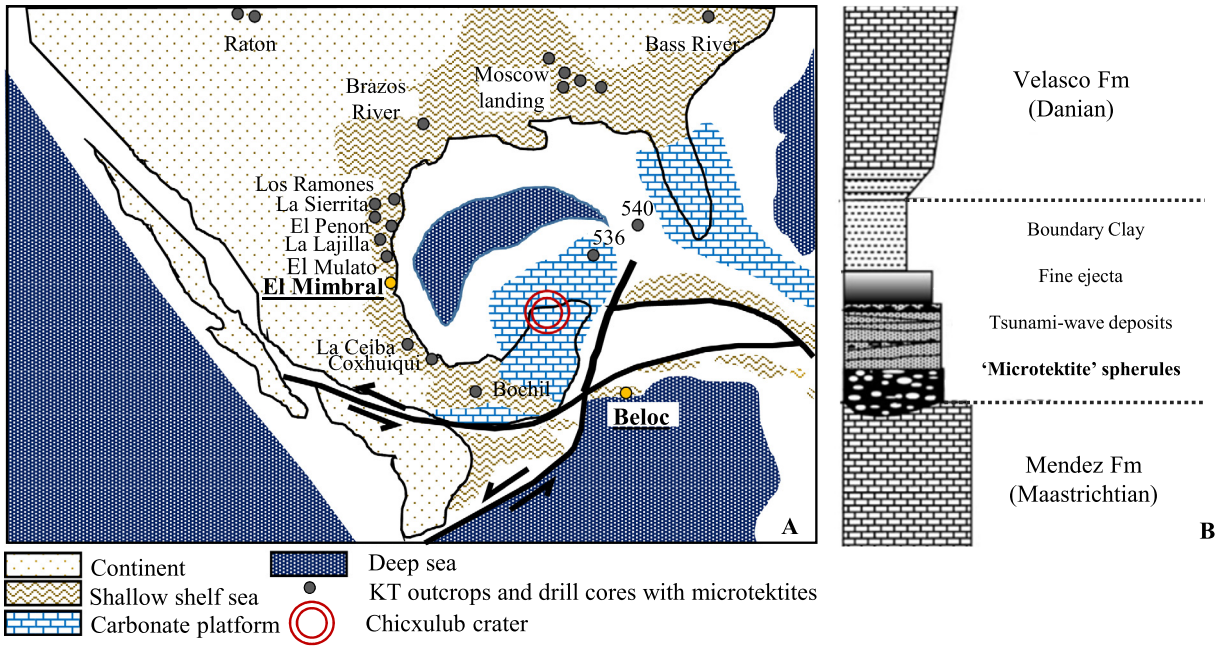

Fig. 1. (A) Paleogeographic map (66 Ma) showing the location of the Chicxulub crater (red circle), DSDP sites 540 and 536 and proximal K–Pg settings including Arroyo El Mimbral and Beloc (redrawn from Smit, 1999). (B) Simplified stratigraphic column of proximal K–Pg settings (modified from Smit, 1999). Spherules are located at the base of impact-induced tsunami-wave and oscillatory wave deposits and are physically separated from the PGE-enriched Boundary Clay layer. (For interpretation of the references to color in this figure legend, the reader is referred to the web version of this article.)

spectroscopy, this study attempts to elucidate the origin and formation mechanism of microtektite spherules at proximal K–Pg settings. In addition, the geochemical and textural relationships between the original glass composition and alteration products are explored. Understanding the alteration patterns of glasses in relation to their precursor material and the diagenetic environment to which these were exposed is crucial in unraveling original melt compositions at localities where relict impact glass phases are lacking.

3.1. Samples

We examined spherules from two localities for which glass has been reported to be abundant, in two opposite quadrants from the source crater: the Arroyo El Mimbral locality (North Eastern Mexico) and the Beloc locality (Jacmel highway, Southern Peninsula of Haiti) (Fig. 1). Samples from Arroyo El Mimbral and Beloc were collected by Ph.C. and J.S. during field trips in the mid-90s and subsequently stored at the Vrije Universiteit Brussel (VUB) and Vrije Universiteit (Amsterdam). At both localities, spherules commonly occur as perfectly round spheres and elongated ellipsoids, although other shapes, such as dumbbells, teardrops and fused ('twin') spherules are present as well. Spherule size varies between 1 and 8 mm. Spherules make up less than 80 vol% of the total deposit and are set in a matrix of marl that contains rounded carbonate clasts, relic foraminifera, and large, irregularly shaped vesicular melt particles with a vitroclastic texture.

At the Beloc locality, glass was found to be abundantly present. Spherules were handpicked from the loose marly deposit and gently fragmented to expose the glass cores. Glass fragments were ultrasonically cleaned with 18 Ω cm - milli-Q H_2O. At Mimbral, high amounts of $CaCO_3$ locally seem to have cemented large parts of the spherule deposits. Here, a more rigorous sample processing was carried out to concentrate relict glass present in the spherules. Rock pieces were gently crushed down to 1 cm sized chips, and individual spherules were handpicked out of the debris. In total, around 10,000 spherules were recovered. Several batches of the separated spherules were soaked in dilute acetic acid (10 vol%) for 24 h to remove the carbonate fraction, and subsequently disaggregated by ultrasonication (1 h at room temperature) to peel off the smectite spherule rims. Next, the released fraction was sieved (63 μm mesh diameter) and washed with 18 MΩ cm milli-Q water. The residue was carefully screened for remaining glass pieces under binoculars. In total, around 100 pristine microtektite glass fragments were extracted from the recovered batch. Glass samples from both localities were carefully embedded in epoxy resin (Epofix) and gently polished with SiC paper and diamond paste until a fresh and very smooth surface was exposed. Simultaneously, rock chips and individual spherules were preserved and thin sections were prepared to study the spherules in relation to the deposit from where they were extracted.

3.2. Petrography and major element analysis

Small-scale petrographic features in the glass and surrounding alteration phase were revealed using scanning electron microscopy (SEM) at the Department of Electrochemical and Surface Engineering (VUB) using a JEOL model JSM6400 and a JEOL JSM-7000F field emission SEM unit. Quantitative major elemental analysis was carried

out at the *CAMPARIS* Center for Microanalysis at the *University* of Paris VI (*Pierre* et Marie Curie) using a *CAMECA* SX 100 electron microprobe and wavelength-dispersive X-ray spectrometry. Instrumental parameters used include a spot size of 15 μm, an accelerating voltage of 15 keV, and a beam current of 4 nA. Typical detection limits are in the range of 0.03–0.08 wt% for major elements. Limits of detection (LOD's) and instrumental precision expressed as two times standard deviation are listed in Tables 1 and 2.

3.3. Iron oxidation state

In an exploratory stage, the oxidation state of the iron present in the microtektite glasses was determined by electron probe micro-analysis (EPMA) by measuring the self-absorption-induced shift of the Fe$L\alpha$-peak (see Fialin et al., 2001, for details). For each sample, 10 replicate measurements were carried out using a beam size of 15 μm, a beam current of 20 nA, and an accelerating voltage of 15 keV. Analyses were restricted to glasses containing an FeO_T content of more than 3.5 wt%, as low iron concentrations cause a large uncertainty in the Fe$L\alpha$ peak position (Fialin et al., 2001).

3.4. Raman spectroscopy

Raman spectra from various glass chips and particular alteration products were obtained using a LabRAM HR Evolution (HORIBA Scientific) confocal Raman microscope equipped with a high stability confocal microscope with XYZ motorized stage, 10×, 50×, 100×–50× (WD = 10.6 mm) objectives and a multichannel air-cooled CCD detector (spectral resolution <1 cm^{-1}, lateral resolution 0.5 μm, axial resolution 2 μm), at the Research Group of Electrochemical and Surface Engineering at the VUB. Materials were excited with a 532 nm solid-state laser at a laser power of ~27.5 mW. All analyses were made with a 50× long working distance objective and an acquisition time of 30 s. Peak positions were determined and baseline corrections done using the LabSpec software and the line-type correction.

3.5. LA-ICP-MS

3.5.1. Trace element spot drilling

Trace elements in selected spherules and surrounding alteration phases were assayed using a New Wave Research UP193HE ArF* excimer-based laser ablation system equipped with a standard circular ablation cell and coupled to an Element XR (Thermo Scientific) double-focusing sector field ICP-mass spectrometer at the Department of Analytical Chemistry of Ghent University. Helium was used as the carrier gas to flush the ablation cell and to transport the ablation-generated aerosols to the plasma. Before entering the plasma, He was mixed with Ar in a ratio of 0.5–1. Oxide formation was monitored using the ThO^+/Th^+ ratio while ablating the NIST SRM 612 glass reference material. The extent of oxide formation was always less than 0.6%. Each sample was ablated for 10 s using a laser spot size of 55 or 100 μm. The total acquisition time varied between 90 and 120 s. Time-resolved spectra were processed offline and a background subtraction was applied. Net signals were normalized to ^{29}Si and ^{44}Ca (as determined by EMPA) as internal reference standards to correct for variations in sensitivity due to matrix effects, instrument drift, and different ablation parameters. Quantification was achieved through external calibration against five certified reference standards NIST SRM 612, USGS BHVO-2G, USGS BIR-1G, USGS GSD-1G and USGS GSE-1G. The use of multiple external reference standards ensures that sample concentrations are bracketed by two or more reference standards, thereby limiting the propagation of measurement uncertainties if extrapolated to concentrations too high or too low. For each element, calibration curves were constructed plotting $c^J_{rm}/c^{Int\ Std}_{rm}$ versus $cps^J_{rm}/cps^{Int\ Std}_{rm}$, with c^J_{rm} and $c^{Int\ Std}_{rm}$ the concentration of the analyte element J and the concentration of the internal standard ^{29}Si or ^{44}Ca in the reference material; cps^J_{rm} and $cps^{Int\ Std}_{rm}$ are net count rates for the analyte element J and the internal standard ^{29}Si or ^{44}Ca. All calibration curves yield regression statistics with squared correlation coefficients (R^2) better than 0.985. Over 100 point analyses were performed on selected glass chips, surrounding alteration products, and zones within individual spherules. Limits of detection (LODs) were calculated as three times the standard deviation using repeated analyses of the NIST SRM 612 reference glass. LODs were found to be unstable and varied significantly over the six-month period during which the analyses were carried out. This is the result of matrix effects, variations in ablation yield, changes in the level of interferences, and fluctuations in instrument performance. Average detection limits for most trace elements are at the sub-ppm level and vary in the range of 0.2–0.5 μg/g for most REEs, 1 μg/g for LILE, 0.2–0.5 μg/g for HFSEs and 0.01–0.05 μg/g for PGE. The precision of the measurements was calculated as percent relative standard deviation (%RSD) for each element and typically falls within 5–10%. LA-ICP-MS trace element data of glasses and alteration phases at Beloc and Arroyo El Mimbral are given in Table 3 and Table 4.

3.5.2. 2-dimensional element mappings

To visualize trace element distributions in both glasses and alteration phases, two-dimensional LA-ICP-MS elemental distribution maps were constructed using a line-scan method. During measurement, the sample was moved continuously under the laser along a series of parallel, adjoining, and equally long lines using a spot size of 15 μm. After drilling a line, the laser returned to the same side of the line with an offset of 15 μm and the orientation of the lines perpendicular and in the same direction as the glass-flow trajectory (Ulrich et al., 2009). Selected elements (Mg, Ca, Ti, Fe, Ni, Rb, Sr, Zr, Nb, Ba, La, Ce, Nd, Hf) were chosen for mapping, based on their specific behavior during alteration processes (mobile versus immobile), their geochemical affinity towards a specific phase, and the relative ease to determine their concentrations with LA-ICP-MS. Image processing was performed using the Interactive Data Language software of ITT Visual Information Solutions (Boulder, CO, USA). In this context, it should be noted that a 15 μm spot size limits the spatial resolution. However, it is the best compromise between a sufficiently low LOD (the sensitivity varies with r^2) and lateral resolution. Element maps are expressed in

Table 1
Major element composition of various glasses from Beloc (Haiti) and Arroyo El Mimbral locality (NE Mexico) as determined with electron probe microanalysis (EPMA).

Typical LOD	Oxide wt%	Mimbral green glass			Mimbral red glass			Mimbral black core			Mimbral black glass			Beloc black glass			Beloc yellow glass		
		Average ($n = 27$)	2σ	Recalc 100%	Average ($n = 3$)	2σ	Recalc 100%	Average ($n = 3$)	2σ	Recalc 100%	Average ($n = 17$)	2σ	Recalc 100%	Average ($n = 16$)	2σ	Recalc 100%	Average ($n = 6$)	2σ	Recalc 100%
0.03	Na_2O	2.50	±0.32	2.83	3.17	±0.36	3.61	1.89	±0.28	2.12	3.21	±0.37	3.26	3.41	±0.38	3.45	1.43	±0.25	1.45
0.06	SiO_2	59.3	±0.71	67.1	61.2	±0.73	69.8	58.0	±0.71	65.2	61.3	±0.73	62.2	64.2	±0.75	64.9	47.9	±0.54	48.5
0.05	Al_2O_3	14.4	±0.34	16.2	15.2	±0.35	17.3	14.5	±0.35	16.3	15.3	±0.36	15.5	14.4	±0.35	14.5	12.4	±0.32	12.6
0.04	MgO	2.26	±0.14	2.56	0.29	±0.06	0.33	2.51	±0.16	2.83	3.47	±0.19	3.52	2.75	±0.17	2.77	4.94	±0.23	5.01
0.04	K_2O	0.86	±0.19	0.97	0.84	±0.19	0.96	0.78	±0.19	0.87	1.41	±0.25	1.43	1.59	±0.27	1.61	0.34	±0.13	0.34
0.03	CaO	3.91	±0.34	4.42	3.49	±0.33	3.98	5.46	±0.41	6.14	6.76	±0.46	6.86	6.45	±0.45	6.51	24.7	±0.83	25.0
0.04	TiO_2	0.69	±0.18	0.78	0.80	±0.19	0.91	0.69	±0.18	0.77	0.73	±0.19	0.74	0.59	±0.17	0.59	0.52	±0.17	0.53
0.08	MnO	0.08	±0.12	0.10	<LOD	<LOD	<LOD	0.10	±0.12	0.11	0.14	±0.13	0.14	0.13	±0.12	0.13	0.11	±0.13	0.11
0.11	*FeOT	4.35	±0.35	4.92	2.24	±0.31	2.56	4.94	±0.47	5.55	6.06	±0.53	6.15	5.15	±0.48	5.20	5.54	±0.50	5.61
0.04	P_2O_5	0.07	±0.03	0.07	0.10	±0.04	0.11	<LOD	<LOD	<LOD	0.10	±0.04	0.10	0.27	±0.04	0.27	0.20	±0.05	0.20
0.04	SO_2	<LOD	<LOD	<LOD	<LOD	<LOD	<LOD	<LOD	<LOD	<LOD	<LOD	<LOD	<LOD	<LOD	<LOD	<LOD	<LOD	<LOD	<LOD
0.09	Cr_2O_3	<LOD	<LOD	<LOD	<LOD	<LOD	<LOD	<LOD	<LOD	<LOD	<LOD	<LOD	<LOD	<LOD	<LOD	<LOD	<LOD	<LOD	<LOD
	Total	88.4		100.00	87.69		100.00	88.94		100.00	98.54		100.00	99.03		100.00	98.65		100.00

*FeOT, total iron measured as FeO.
n, number of spot analyses.
2σ, instrumental precision.
LOD, limit of detection.

Table 2
Major element composition of alteration phases from Beloc (Haiti) and Arroyo El Mimbral locality (NE Mexico) as determined with Electron Probe Microanalysis (EPMA).

Typical LOD	Oxide wt%	Beloc rim L1 ('palagonite')		Beloc rim L2 ('smectite')		Mimbral spherule rim		Mimbral corrosion green glass		Mimbral alteration red glass		Mimbral orange fragments		Mimbral K-rich 'shards'	
		Average ($n = 1$)	2σ	Average ($n = 4$)	2σ	Average ($n = 9$)	2σ	Average ($n = 2$)	2σ	Average ($n = 2$)	2σ	Average ($n = 4$)	2σ	Average ($n = 2$)	2σ
0.03	Na_2O	0.11	±0.08	0.03	±0.09	0.05	±0.09	0.06	±0.11	0.15	±0.11	0.07	±0.09	<LOD	<LOD
0.06	SiO_2	46.8	±0.65	57.6	±0.71	41.6	±0.61	36.3	±0.57	41.3	±0.61	51.6	±0.68	52.2	±0.68
0.05	Al_2O_3	23.9	±0.49	16.3	±0.38	15.0	±0.37	11.4	±0.32	14.3	±0.36	23.3	±0.48	25.2	±0.50
0.04	MgO	0.34	±0.07	5.61	±0.23	9.24	±0.31	14.6	±0.40	11.4	±0.35	0.30	±0.07	2.79	±0.16
0.04	K_2O	0.14	±0.10	0.34	±0.13	0.39	±0.14	0.32	±0.13	0.38	±0.13	0.08	±0.09	5.86	±0.60
0.03	CaO	1.73	±0.23	2.59	±0.28	2.75	±0.29	0.92	±0.18	2.18	±0.26	3.01	±0.30	0.85	±0.17
0.04	TiO_2	0.81	±0.19	0.84	±0.19	0.09	±0.11	0.76	±0.18	0.53	±0.16	1.21	±0.22	0.14	±0.11
0.08	MnO	<LOD	<LOD	<LOD	<LOD	<LOD	<LOD	0.15	±0.13	0.19	±0.14	<LOD	<LOD	<LOD	<LOD
0.11	*FeOT	11.2	±0.75	6.76	±0.56	17.9	±0.94	23.4	n.d.	16.5	±0.86	7.97	±0.61	3.32	±0.38
0.04	P_2O_5	<LOD	<LOD	<LOD	<LOD	0.04	±0.03	0.05	±0.03	<LOD	<LOD	<LOD	<LOD	0.04	±0.03
0.04	SO_2	0.04	±0.02	0.04	±0.02	<LOD	<LOD	<LOD	<LOD	<LOD	<LOD	<LOD	<LOD	<LOD	<LOD
0.09	Cr_2O_3	<LOD	<LOD	<LOD	<LOD	<LOD	<LOD	<LOD	<LOD	<LOD	<LOD	<LOD	<LOD	<LOD	<LOD
	Total	85.03		90.17		87.09		88.02		86.90		87.59		90.42	

n.d., not determined.
*FeOT, total iron measured as FeO.
n, number of analyses.
LOD, limit of detection.

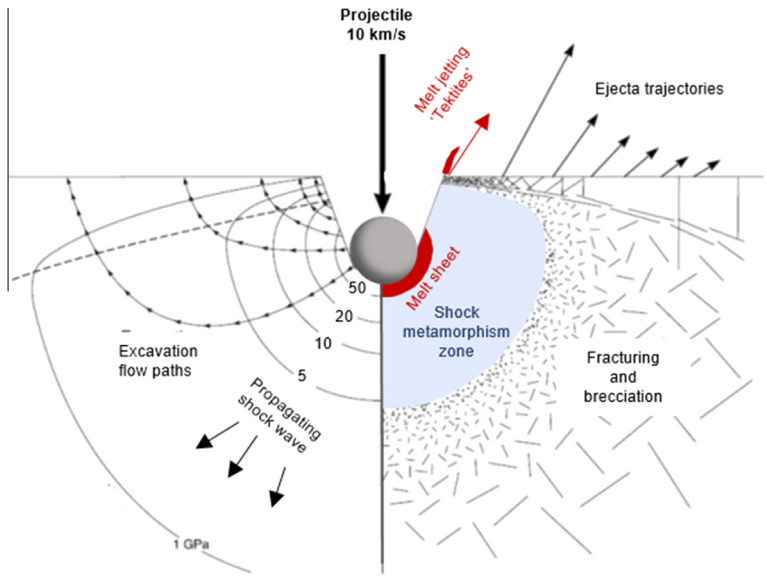

Fig. 2. Postulated formation mechanisms for impact glasses. Glassy spherules from Chicxulub are termed 'microtektites'. Tektites are thought to have formed from the uppermost layers of the target in the early stages of the cratering process. However, K–Pg microtektites stem from a deeper part of the target. Microtektites are more likely to be expelled from the central melt sheet (image modified after French, 1998).

counts per seconds for a maximum daily count rate. Details about the mapping procedure and image processing can be found in Izmer et al. (2013).

3.6. Whole rock trace element analysis using acid digestion and solution ICP-MS

Four whole-rock batches of the spherule beds at Mimbral and Beloc were measured for trace element composition after classical wet chemistry sample pretreatment. Sample sets include a batch from Beloc whole rock (BWR), Mimbral whole rock (MWR), Mimbral individual spherules (MSph), and Beloc glass (BGL). Samples were manually ground using an agate mortar and pestle. Approximately 100 mg of sample powder was accurately weighed in pre-cleaned acid-resistant Teflon® vials and digested following the procedure of Goderis et al. (2010). Certified reference standards BE-N (Centre National de la Recherche Scientifique – CNRS), PM-S (CNRS), PCC-1 (United States Geological Survey – USGS), and the in-house standard SK-10 as well as one procedural blank were subjected to the same analytical protocol. The measurement of selected trace elements was carried out using a quadrupole-based Thermo Scientific XSeries II ICP-MS instrument at the Department of Analytical Chemistry at Ghent University. Instrumental precision expressed as percent relative standard deviation is in the range of 0.5–2%.

4. RESULTS

4.1. Spherules and extracted microtektite glass fragments: morphological and petrographic characteristics

4.1.1. Beloc

At Beloc, glass spherules are pseudomorphically transformed into a brown Fe–Mg alteration product qualified as 'smectite' by several authors (Izett, 1991a,b; Koeberl and Sigurdsson, 1992; Glass and Simonson, 2012). However, Bohor and Glass (1995) emphasize the presence of both poorly crystalline smectite and 'palagonite'. Palagonite has been used as a descriptive term to denote yellow and brown alteration products of basaltic glass (Berkgaut et al., 1994). Palagonite forms as a poorly crystalline product following initial hydration of the glass, before crystallization into smectite. The extent to which the glass is preserved within the alteration shell varies. Spherules that do not host a remnant glass core are completely replaced by massive 'smectite'. Contrarily, in some spherules, the replacement is not completed. Here, a remnant glass core can still be observed. In such spherules in which the glass is still preserved and where it can be observed in direct association with its alteration products, it can be seen that this 'smectite' rim surrounding the pristine glass is in fact composed of two distinct zones: an outer brown zone (L2) and an inner yellowish-white zone (L1), present directly at the interface with the corroded glass surface (Fig. 3I). This double-layered alteration rim exhibits convex-shaped articulations gradually penetrating the glass (Figs. 3I and 4A–C). Bohor and Glass (1995) interpreted this as an expression of the hemispherical shape of hydration fronts growing inward from point sources near the spherule's original surface. Separated microtektite glass fragments display a pitted, scalloped outer surface (Fig. 5A), the 'cast' of the mammillary inner surface constituting the surrounding alteration layer (Bohor and Glass, 1995). A detailed investigation of the spherule alteration layers was done with FEG-SEM. Fig. 5C shows an example of the outer brown alteration zone L2 in a typical 'cellular' or 'honeycomb' texture indicating early diagenetic formation of smectite (Keller et al., 1986). The yellow

Table 3
Trace element composition of various glasses from Beloc (Haiti) and Arroyo El Mimbral locality (NE Mexico) as determined with LA-ICP-MS.

(μg/g)	Mimbral green glass Average ($n = 30$)	Mimbral red glass Average ($n = 4$)	Mimbral black core Average ($n = 4$)	Mimbral black glass Average ($n = 12$)	Beloc black glass Average ($n = 61$)	Beloc yellow glass Average ($n = 13$)
Sc	21.8	19.6	26.4	26.7	20.2	16.1
V	137	144	140	175	110	112
Cr	83.3	85.7	91.3	104	44.1	49.2
Co	10.8	4.32	15.4	17.9	9.50	14.0
Ni	20.0	20.9	27.7	31.7	29.4	35.1
Cu	1.31	1.37	<LOD	35.3	27.9	35.4
Zn	97.3	206	n.a.	75.4	82.8	167
Ga	15.1	15.1	n.a.	17.8	15.2	14.5
Ge	<LOD	1.05	n.a.	2.00	1.51	4.17
As	<LOD	<LOD	n.a.	<LOD	<LOD	8.46
Rb	30.6	29.4	30.2	47.6	45.3	14.6
Sr	2035	5244	624	380	449	1629
Y	20.0	18.6	19.7	25.7	22.3	19.1
Zr	102	94.2	95.0	130	132	96.5
Nb	5.1	4.9	4.7	6.0	6.1	5.4
Cs	8.86	17.9	n.a.	1.13	0.99	0.17
Ba	1100	2066	469	416	558	361
La	15.3	13.2	14.6	19.2	19.6	19.0
Ce	32.1	28.9	30.0	38.8	41.2	39.7
Pr	3.85	3.46	3.79	4.72	4.93	4.71
Nd	12.1	14.3	13.8	15.4	18.4	17.6
Sm	3.63	3.22	3.71	4.90	4.38	4.00
Eu	1.00	0.87	0.96	1.14	1.22	1.12
Gd	3.46	3.10	3.39	5.14	4.07	3.74
Tb	0.52	0.58	0.59	0.71	0.65	0.57
Dy	3.66	3.57	3.39	5.20	4.16	3.87
Ho	0.75	0.63	0.65	1.00	0.88	0.76
Er	2.15	2.04	1.73	2.80	2.45	2.20
Tm	0.33	0.32	0.27	0.45	0.39	0.36
Yb	2.27	2.00	2.26	2.91	2.70	2.27
Lu	0.35	0.24	0.35	0.56	0.40	0.31
Hf	3.33	2.93	2.63	4.57	3.96	2.74
Ta	0.38	0.32	0.31	0.41	0.42	0.36
W	0.88	0.69	0.54	0.79	0.69	2.14
Ir	<LOD	<LOD	<LOD	<LOD	<LOD	<LOD
Pt	<LOD	<LOD	<LOD	<LOD	<LOD	<LOD
Au	<LOD	<LOD	<LOD	<LOD	<LOD	<LOD
Pb	4.73	12.0	2.25	3.29	4.38	9.18
Th	5.54	4.37	5.04	7.33	6.33	5.10
U	1.42	1.23	1.10	1.85	1.40	2.28

n.a., not detected.
LOD, limit of detection.
n, number of analyses from which the average was calculated.

layer L1 is composed of a poorly crystalline material, high in Al and Fe (Fig. 5B) and may correspond to palagonite, a precursor of the well-crystallized smectite alteration rim.

Amongst the relict glass cores, black glass represents the most abundant variety. The yellow type glass is only present as schlieren or small patches admixed in various proportions within the black glass (Fig. 4A–C).

4.1.2. Arroyo El Mimbral

Spherules from Arroyo El Mimbral are morphologically similar to those at Beloc, although a greater proportion appears reworked, broken, and often plastically deformed as a result of post-depositional burial and compaction. Alteration features of the spherules vary throughout the deposit. In the marly fractions, spherules are mostly altered into a Fe–Mg rich phase with a composition similar to smectite/chlorite (Fig. 6) according to qualitative energy dispersive spectrometry. Although the style of alteration is similar to observations made for Beloc, the secondary replacement is not massive, but zoned. In most spherules, several parallel concentric alteration lamellae are lined with finely dispersed Fe–Ti precipitates (Fig. 7A and B). In addition, the composition of the spherule rim may vary from mixed smectite–chlorite to chlorite. The inner parts of the spherules are filled with diagenetic blocky calcite.

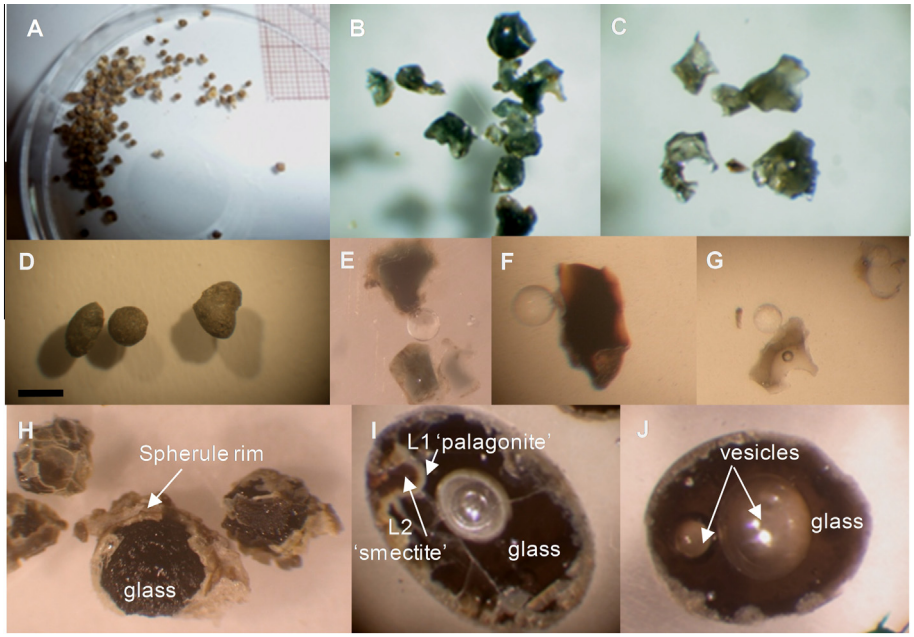

Fig. 3. (A and D) Spherules separated from the Arroyo El Mimbral locality. Green glass fragments represent the most abundant variety, followed by black glass. (B and C) Note scalloped nature of the glass fragments. (E–G) Polished green (E), red (F) and black glass (G) from Mimbral. (H) Spherules from Beloc showing black glass core in the center of an alteration shell. (I and J) Polished cuts from Beloc spherules with glass core. In some spherules a double-layered alteration rim, consisting of gel-like 'palagonite'(L1) and 'smectite' (L2) can be observed. Note the presence of large vesicles in the center of the spherules. (For interpretation of the references to color in this figure legend, the reader is referred to the web version of this article.)

In the more carbonate-rich parts of the deposit, spherules are almost completely replaced with secondary calcite and display only a thin (~20 μm) Fe–Mg alteration rim. Bubble cavities are lined with smectite/chlorite and filled with calcite as well. Interestingly, calcite-replaced spherules often host altered K-rich, (partially) isotropic fragments (Figs. 7C, D and 8A–D) with low analytical totals determined by microprobe. Morphologically, these fragments resemble the scalloped pristine glass pieces extracted from the same spherule deposit (Fig. 3B and C). Interestingly, these K-rich shards show circular cracks (Fig. 8B and D) that are strikingly similar to perlitic fractures formed during hydration of high-SiO_2 volcanic glass (Fig. 8E–G). Such typical perlite fabric is formed when water is introduced into glass causing it to expand (Friedman and Smith, 1958). Subsequently, the glass surface cracks when large tensile stress exceeds the mechanical strength of the glass (Meisinger, 1980).

At Mimbral, relict glass is extremely scarce. From a total of 10,000 spherules, only 100 (small) glass pieces were extracted. Glass fragments are characterized by a scalloped surface (Fig. 3B and C) and range in size from 70 to 300 μm. The fragments display a variety of color, ranging from green to red and black. The green glass is the most abundant variety, followed by black and red glass type. Green glass chips often contain a black glass core (Fig. 4G and H). Although yellow glass has also been reported for this location (Blum et al., 1993; Claeys et al., 1993; Premo et al., 1995), no yellow glass was found in this work. Due to extensive processing to separate the glass out of the spherules, only two black glass particles were found with the alteration phase still attached to the glass. The alteration phase consists of a yellowish, semi-translucent phase high in Al and Fe with a composition strikingly similar to the first L1 ('palagonite') alteration layer at Beloc. Apart from the glass fragments, some yellow-orange, partially isotropic particles were found in the residue as well (Fig. 9A). These shards have a convex-shaped morphology and a composition similar to the Al–Fe rich L1 ('palagonite') alteration layers surrounding relict glass cores both at Beloc and Arroyo El Mimbral. In addition, the shards show a striking resemblance with palagonitized volcanic glass fragments reported in literature (Fig. 9B).

Because of the scarcity of the glass at the Arroyo El Mimbral locality and extensive sample processing, it was extremely difficult to find a glass fragment in direct association with its host spherule. From the batch of spherules that was kept intact and for which the spherules were embedded in Epoxy resin as a whole, only two (green) pristine glass fragments were found, present as relict, scalloped glass cores in the center of a calcite-replaced spherule (Fig. 8H–J). Interestingly, from the batches of processed spherules from which glass fragments were extracted, the greatest abundance of glass fragments is in fact found in the batch of calcite-replaced spherules. Glass particles are often broken and show conchoidal fractures (Fig. 10D). Some green glasses show Fe(Mg)-rich corrosion products at the surface (Fig. 10A–C, E, F). SEM images indicate these consist of lath-shaped corrosion products gradually penetrating the glass along microfractures (Fig. 10E). Mazer et al. (1992) emphasize that the penetration of clay

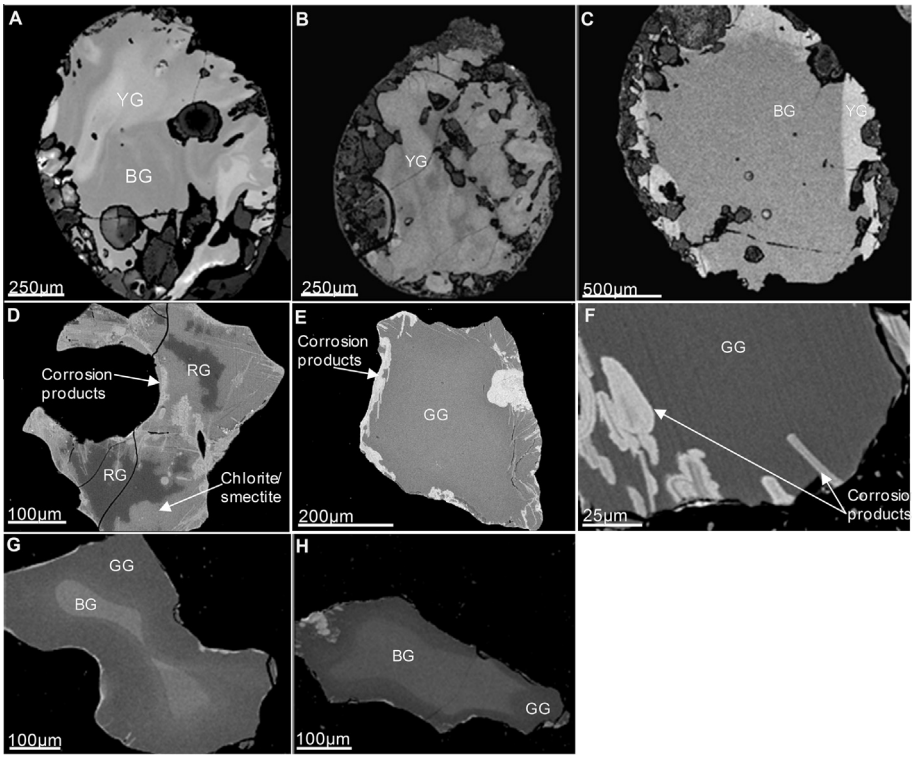

Fig. 4. Back-scattered electron images. Top row (A–C): whole spherules with large glass core surrounded by an alteration rim extracted from Beloc locality. Note high contrast zones marking the compositional variation within the glass. High contrast zones represent Ca (and S-) rich yellow glass (YG) admixed in various proportions within the black glass (BG). Lower rows: glass fragments separated out of spherules from Arroyo El Mimbral. (D) Red glass (RG, darkest zones) surrounded by a chlorite alteration layer (light zones) and penetrated by Fe(Mg)-rich corrosion products (high contrast zones). (E and F) Green glass fragments (GG); high contrast zones are (Fe)Mg-rich corrosion products. (G and H) Green glasses (GG) often host black glass (BG) cores low in Si.

laths into glass suggest *in situ* hydrolysis of the glass network followed by restructuring to form clay-rich mineral. Two types of alteration products surround the red glass (Fig. 4D). The glass core has a Fe–Mg alteration layer with a composition that mirrors that of the spherule alteration rims at Arroyo El Mimbral (Table 2). At the edges, Fe(Mg) corrosion products penetrate the glass surface. These corrosion products have a composition similar to the corrosion products found in association with the green glasses from Mimbral (Table 2).

4.2. Major element composition of the glass and alteration products

A striking observation is that all (and only) green and red glasses at Arroyo El Mimbral have electron microprobe totals significantly below 100 wt% oxides (85–90 wt%), suggesting the presence of H_2O (Table 1). In addition, the green glass appears more friable and sensitive to beam-damage compared to non-hydrated black glass with a similar thickness. Nonetheless, low analytical totals were consistently found in repeated analyses for all green and red glasses under varying beam conditions (changing the beam current from 4 to 20 nA and reducing counting time). Raman spectroscopy was used to investigate the presence of water in all tektite groups. Two spectral regions can be distinguished in Raman spectra of hydrated silica glasses (Le Losq et al., 2012): a low wave number region (15–1500 cm^{-1}), corresponding to vibrations of the silicate network, and a high wave number region (3100–3750 cm^{-1}), which relates to OH stretching vibrations of H_2O molecules and OH groups. Green glasses from Mimbral clearly show the characteristics of a hydrated glass (Fig. 11), not an alteration phase. Compared to green and black glass, red tektites from Mimbral show a prominent disappearance of the spectral units related to vibrations of the silicate network, suggesting breakdown of the glass structure. The OH wave number region does not appear in the black and yellow varieties at both Mimbral and Beloc, which is in agreement with their high analytical totals (98–100 wt%, Table 1). All green and red glasses investigated in this study appear to be hydrated (Fig. 11).

To allow comparison between the glass types, all major element compositions as determined by EPMA were recalculated on a 100% water-free basis. When plotting the Na_2O content of the glasses against the total wt% oxide content (Fig. 12), indicative for Na loss during measurement or alkali depletion during alteration and ion-exchange, no significant variation can be observed. Consequently, despite low analytical totals, relative trends in the major element composition should still be representative after normalization on a water-free basis.

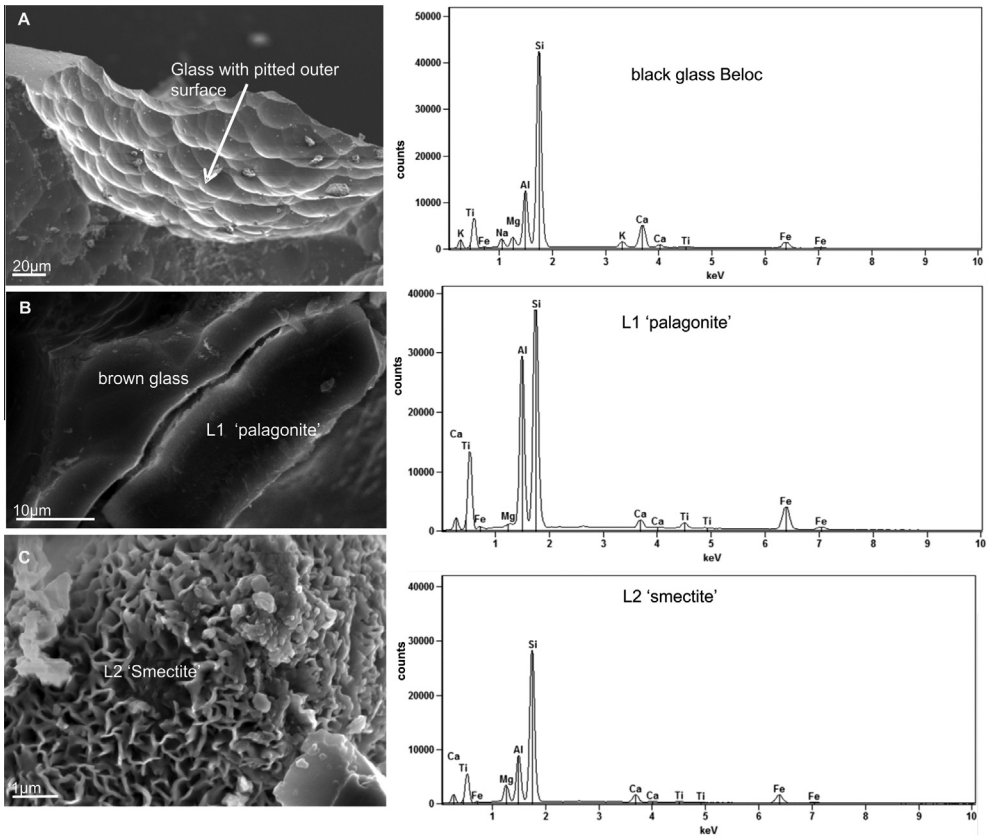

Fig. 5. (A) Secondary electron image of glass fragment from Beloc locality showing pitted outer surface, the cast of the mammillary inner surface of the surrounding alteration layer. (B) Transition from glass to the first alteration layer (L1). Alteration layer is poorly crystalline. (C) Detail of the second alteration layer, showing honey-comb texture typical of early diagenetic smectite. Representative energy dispersive X-ray spectra obtained from polished samples. The L1 layer is characterized by a (relative) increase in Al, Fe and Ti and decrease in Si, Na, K, Ca and Mg. The L2 layer represents a well-crystallized smectite enriched in Mg.

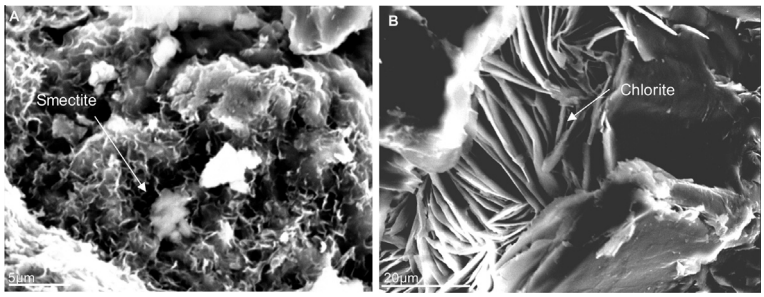

Fig. 6. Secondary electron images from spherule rim at Arroyo El Mimbral locality showing flaky chlorite–smectite like alteration products.

Both in terms of geochemistry and color, green and red, black, and yellow glasses form three distinct groups (Table 1): for Arroyo El Mimbral, green and red glasses are high in SiO_2 (~68–72 wt%), and Al_2O_3 (~16–17 wt%) and low in MgO (~2 wt%), FeO (~4 wt%), and CaO (~4 wt%). Yellow glasses are rich in CaO (~13–24 wt%) and MgO (4–5 wt%) and low in SiO_2 (~36–48 wt%), Al_2O_3 (~11–13 wt%), Na_2O (~0.5–1.5 wt%), and K_2O (~0.1–0.5 wt%). In terms of SiO_2 and Al_2O_3 contents, black glasses have intermediate compositions between yellow and green glasses (SiO_2 ~60–65 wt%, Al_2O_3 ~15 wt%, Na_2O ~2–4 wt%, K_2O ~1–2 wt%, CaO ~5–8 wt%, FeO ~5–6 wt%; Table 1). Black glass schlieren and cores admixed within the green glass have similar major element compositions as the black glass variety extracted from the same deposit. The black glass variety at Beloc is compositionally indistinguishable from the black glass at Mimbral. Selected major element binary variation diagrams (Fig. 13) show positive correlations of SiO_2 with Al_2O_3, K_2O and Na_2O, and negative correlations with CaO, FeO and MgO for all glass types, with exception of the yellow glass, in which FeO positively correlates with SiO_2. The latter emphasizes

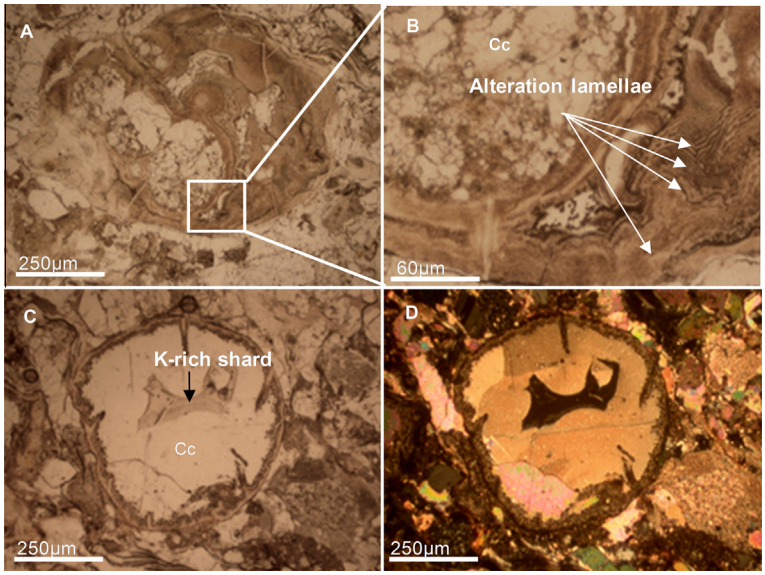

Fig. 7. (A) Thin section micrographs of spherules from Arroyo El Mimbral locality (A, B, C plane polarized light, D crossed polarized light). (A and B) Spherules display a multi-layered alteration rim with fine Fe–Ti oxides that line the multiple alteration lamellae reminiscent of former hydration fronts. (C and D) Spherules are diagenetically filled with blocky calcite (Cc) and host (partially) isotropic K-rich shards which morphologically resemble the scalloped pristine glass fragments extracted from the same deposit.

the dominant control of FeO from a mafic source for the yellow glasses, while the CaO and MgO contents originate from a marine carbonate/dolomite/evaporite source. For the green and black glasses, the CaO content is independent of the FeO content; CaO is almost constant for a given range of FeO contents. At the same time, MgO positively correlates with FeO. The MgO and FeO contents seem to be controlled by the addition of a mafic source, that is more prominent in the black glass compared to the more felsic green glasses which are low in FeO, CaO, and MgO. These observations are consistent with studies by Kettrup and Deutsch (2003), who emphasize the presence of a mafic precursor based on Sr–Nd model ages of impact melts and the presence of mafic target lithologies (amphibolites) among the clasts in the ejecta blanket.

4.3. LA-ICP-MS trace element spot analysis

Despite their distinct major element composition, CI-normalized spidergrams (Figs. 14 and 15) show a striking similarity between green, black, and yellow glasses for most of the trace elements. For the yellow glass, the main differences are a distinctly higher Sr and slightly higher U content, and lower Cs and Rb contents compared to the black glass variety. In addition, REEs exhibit similar upper continental crust patterns, although the yellow glass is relatively depleted in the heavy REEs (HREE) compared to the light REEs (LREE). Interestingly, REEs do not show the expected depletion when the black glass variety (high-Si end member) is mixed with marine carbonate/anhydrite (for which the CI-normalized REE pattern is flat and total REE contents generally very low) in proportions sufficiently high to yield elevated Ca, Mg and S contents. This observation was also made by Koeberl (1993).

A striking observation is that green and red glasses are strongly, but variably enriched in some of the large ion lithophile elements (LILEs) Sr, Ba, and Cs (Figs. 14 and 15). However, these elements do not show a coupled enrichment in Rb. In a CaO versus Sr plot (Fig. 16e), the yellow and black glasses define a positive linear correlation, emphasizing the addition of marine carbonate/evaporite as the source for Sr in both glass types. The Sr content of the green glass does not show a significant systematic variation with the CaO content exhibiting a large range of Sr concentrations for an almost invariable CaO content. Barium shows a slightly positive correlation with K_2O for black and yellow glasses (Fig. 16f). On the contrary, for the green glass, a weak, negative trend is observed between Ba and K_2O. As Sr substitutes for Ca in plagioclase (anorthite) and marine carbonate/sulfate, and Ba for K in K-feldspar, the lack of a clear positive correlation in the green glasses rules out that the Ba and Sr enrichments could be inherent to the source rock. In addition, green glasses do not show a distinct positive Eu anomaly expected from the addition of granitic/pegmatitic (plagioclase-rich) sources generally enriched in Sr and Ba. Strontium shows a strong positive correlation with Cs in the green glass (Fig. 16h). This is also observed for black glasses. Contrarily, the yellow glass is generally very low in Cs and shows a depletion of Cs with increasing Sr content (Fig. 16h). Rubidium is negatively correlated with Sr (Fig. 16i). The yellow glasses show the highest Sr and lowest Rb contents.

In a Ba/Rb versus Rb/Sr plot (Fig. 17), green/red and yellow glasses define two separate trends with the black glass. The green, red, and black glasses fall onto a trend line with end members high and low in Ba and Sr. The yellow glasses plot off this mixing line in a low Rb/Sr field with varying Ba/Rb. Interestingly, yellow and green glass

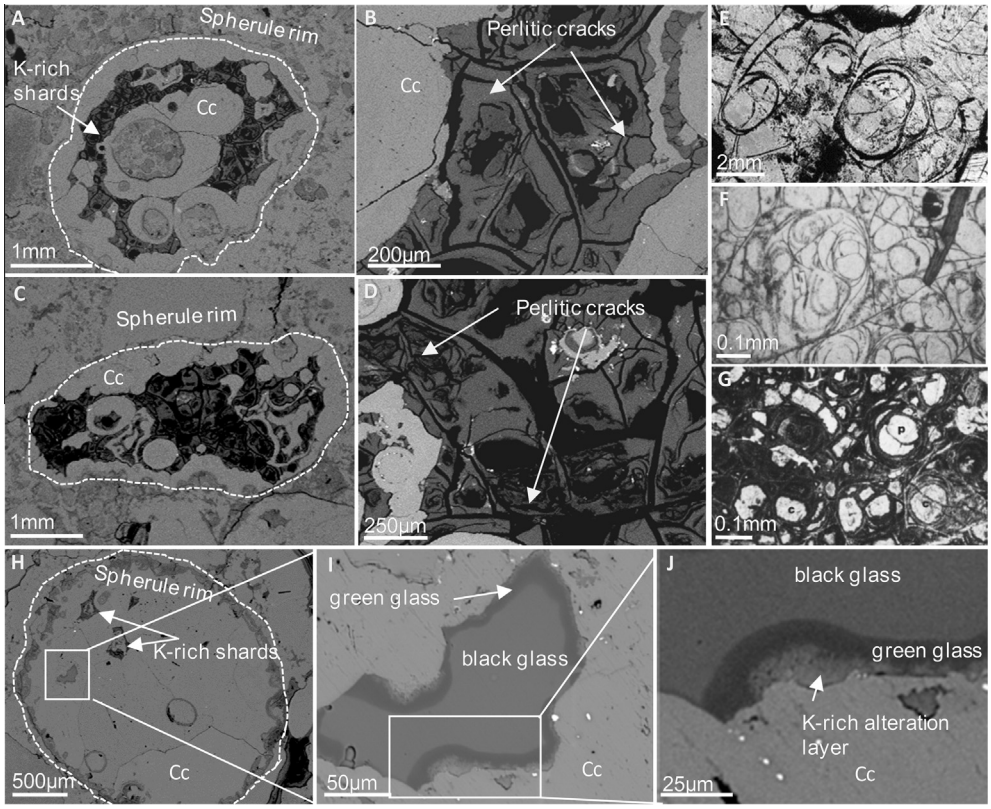

Fig. 8. (A and C) BSE image of calcite-replaced spherules at Arroyo El Mimbral locality. Spherules often host a core of K-rich shards morphologically resembling the scalloped relict glass shards extracted from the same deposit. (B and D) Detail of K-rich shards showing onion-like, gently curved cracks, a fabric typical of perlite which forms upon hydration of high-SiO_2 volcanic glass. (E–G) Thin sections showing characteristic cracks in perlite from altered rhyolitic (high SiO_2) glass for comparison (E image from Heide and Heide (2011); F and G image from Noh and Boles (1989)). (H) BSE image with spherule from Mimbral. The spherule rim is only very thin and the spherule is diagenetically filled with calcite. Small K-rich shards with perlitic cracks are enclosed in the calcite groundmass. The white square shows a pristine glass fragment. (I) Detail of relict glass piece in H showing green high SiO_2 glass with black low SiO_2 core. (J) The rim of the glass seems corroded and consists of corrosion products rich in Fe, Mg and even K.

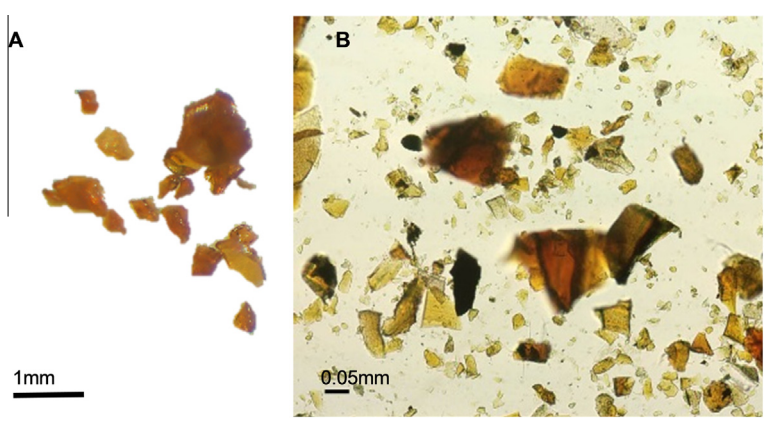

Fig. 9. (A) Yellow semi-translucent fragments extracted from the Arroyo El Mimbral locality. (B) Thin section micrograph showing palagonitized volcanic glass, altered from mafic volcanic glass. Note the striking resemblance with shards extracted from Mimbral locality. Image from Rothwell (1989). (For interpretation of the references to color in this figure legend, the reader is referred to the web version of this article.)

trends converge at the high Ba/Rb end member, suggesting addition from a marine source for both glass types. For the green glass, high Ba, Sr (and Cs) contents are most likely adsorbed from seawater during initial hydration, while for the yellow glass, high Sr and contrasting low Rb and Ba contents are primary and likely originate

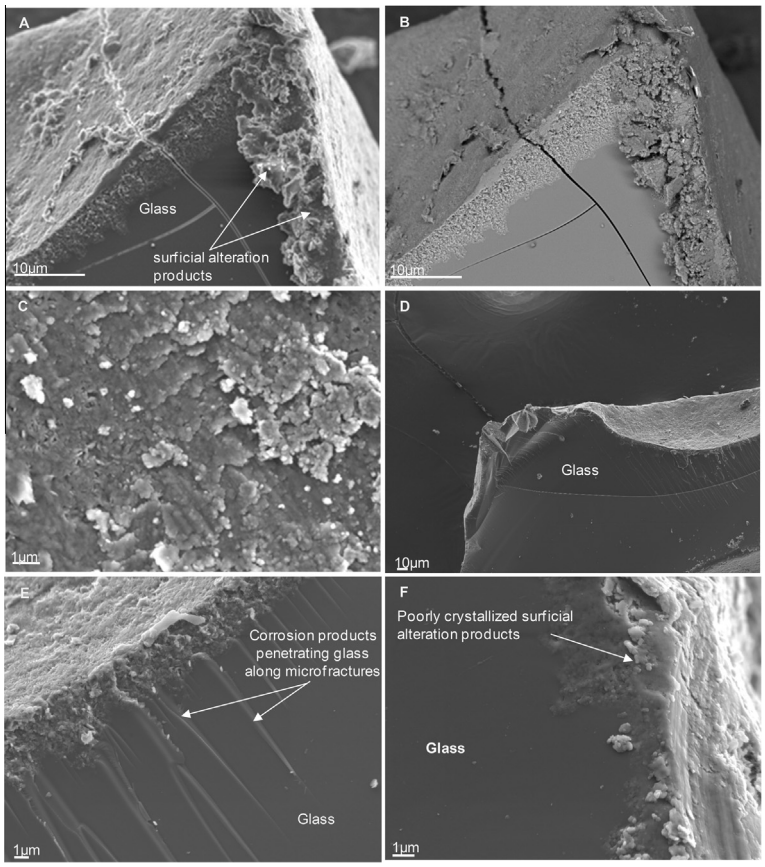

Fig. 10. (A) Secondary electron images from green glass fragments from Arroyo El Mimbral locality. Surface contains Fe–Mg alteration products with a composition typical of chlorite. (B) Back-scattered electron image from the same location as (A) showing the glass-alteration contact. (C) Detail of the surficial alteration products and secondary clay. (D) Conchoidal cleavage exposing fresh glass surface. (E) Note how the lath-shaped alteration products penetrate the glass, indicating *in situ* hydrolysis and replacement by secondary clays. (F) Detail of poorly crystallized surficial alteration products.

from the addition of marine carbonate/evaporite admixed within the melt. A two-component mixing line between black glasses and average seawater composition, plotted in the same Ba/Rb, Rb/Sr diagram, defines a trend opposite to that observed for the green glasses, suggesting a preferred partitioning of alkalis from seawater into the green glass during hydration rather than linear mixing. Addition of seawater alkalis may be supported by Premo et al. (1995) who measured a $^{87}Sr/^{86}Sr$ isotope ratio of 0.70757 for green glasses (with Sr content of 1742 ppm) indicating close resemblance with the ratio of contemporaneous Cretaceous seawater.

Total REE contents are also plotted against SiO_2, CaO and Sr contents (Fig. 16a–c). In the yellow glasses, REE show a clear positive variation with SiO_2 and a negative correlation with CaO, emphasizing the dominant control of the silicate end member enriching and the carbonate end member diluting the total REE budget. For the green glasses, there is no observed systematic variation of the REE neither with the total SiO_2 nor with the CaO content, although the total REE content of green glasses is slightly lower compared to both black and yellow glasses. The lack of a clear variation of the REE content with Sr in the green glasses, which could be a measure for the degree of hydration/seawater adsorption, suggests a rather complex and dynamic interplay between the glass and an evolving fluid composition. Nonetheless, the slight depletion of the REE content in the green glasses, and the slight negative correlation between K and Ba as well as Sr and Ca constitutes an additional argument for the onset of ion-exchange (leaching) during hydration.

Because high field strength element (HFSE) pairs Zr–Hf and Nb–Ta have the same charge (5^+, 4^+) and similar ionic radii, Zr–Hf and Nb–Ta pairs show a similar geochemical behavior during geochemical processes, including alteration. Their ratios (Zr/Hf, Nb/Ta) may be useful in tracing original glass compositions. In addition, HFSE are considered immobile species during aqueous alteration processes. In a Zr/Hf versus Nb/Ta diagram, individual analyses of smectite rim compositions at Beloc resulted in Zr/Hf ratios similar to the adjacent glass phase, although Nb/Ta ratios seem to decrease (Fig. 18). Averaging out the Zr/Hf and Nb/Ta of the L1 layer results in good agreement with the range of the pristine glass compositions. The large scatter in ratios amongst individual spot analyses may be attributed to the targeting of insoluble 'nuggets', residually

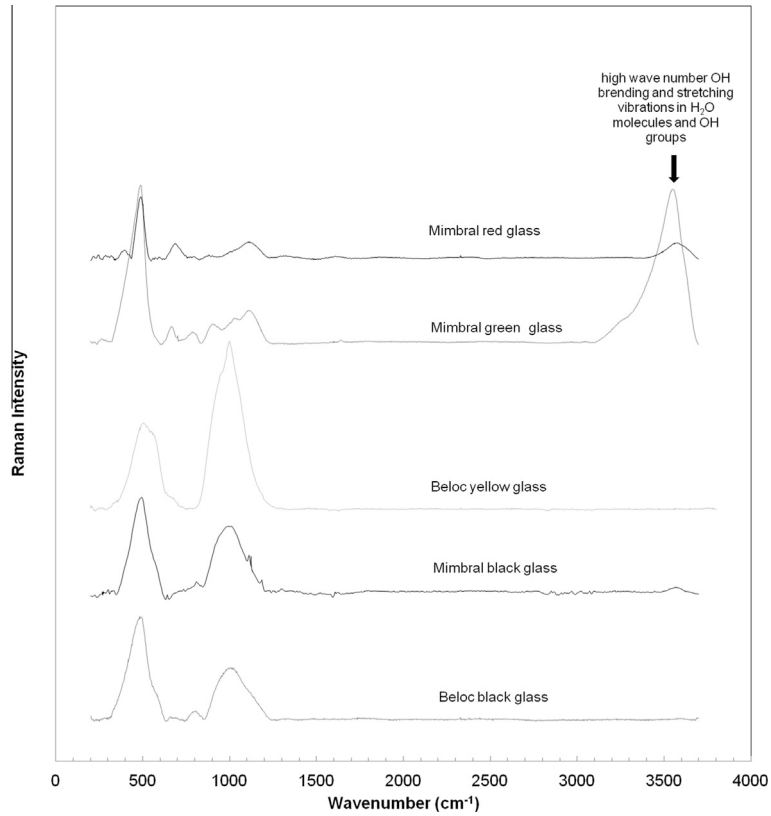

Fig. 11. Representative baseline-subtracted Raman spectra of selected microtektite glass types. Black and yellow glasses display the spectra of a typical glass with characteristic peaks in the 500 and 1000 cm^{-1} region corresponding to bending and stretching vibrations of the silicate network. All green glasses from Mimbral appear hydrated as indicated by the broad band in the 3000–3700 cm^{-1} region corresponding to bending and stretching vibrations of H_2O molecules and OH-groups. Black and yellow glasses from Mimbral and Beloc show the spectra of hydrated glass. The red type glasses seem to represent a more advanced stage in the alteration of the green glass. As alteration proceeds, the green glass develops a broader band in the 1000 cm^{-1} region with a sharp drop in intensity, suggesting leaching of alkalis out of the glass structure. The development of a high peak in the 500 cm^{-1} region suggests increased polymerization due to the formation of new Si–O bonds.

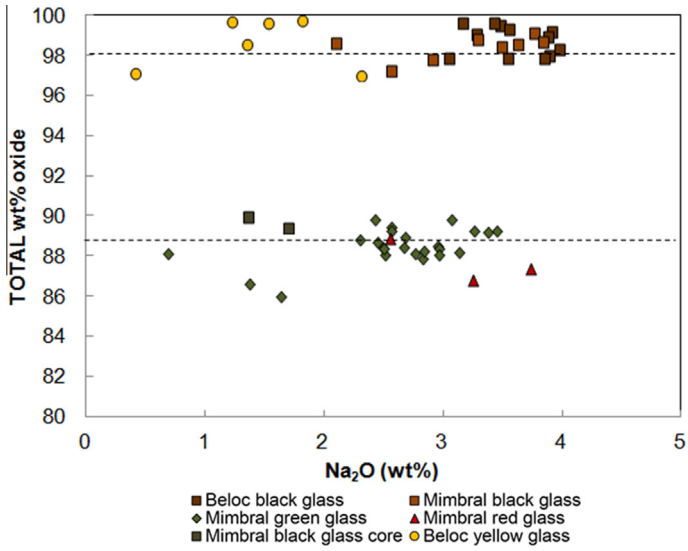

Fig. 12. Plot of total wt% oxide as determined by EMPA versus the Na_2O content of various glasses. There is no significant variation of the Na_2O content with oxide totals for the green glasses. (For interpretation of the references to colour in this figure legend, the reader is referred to the web version of this article.)

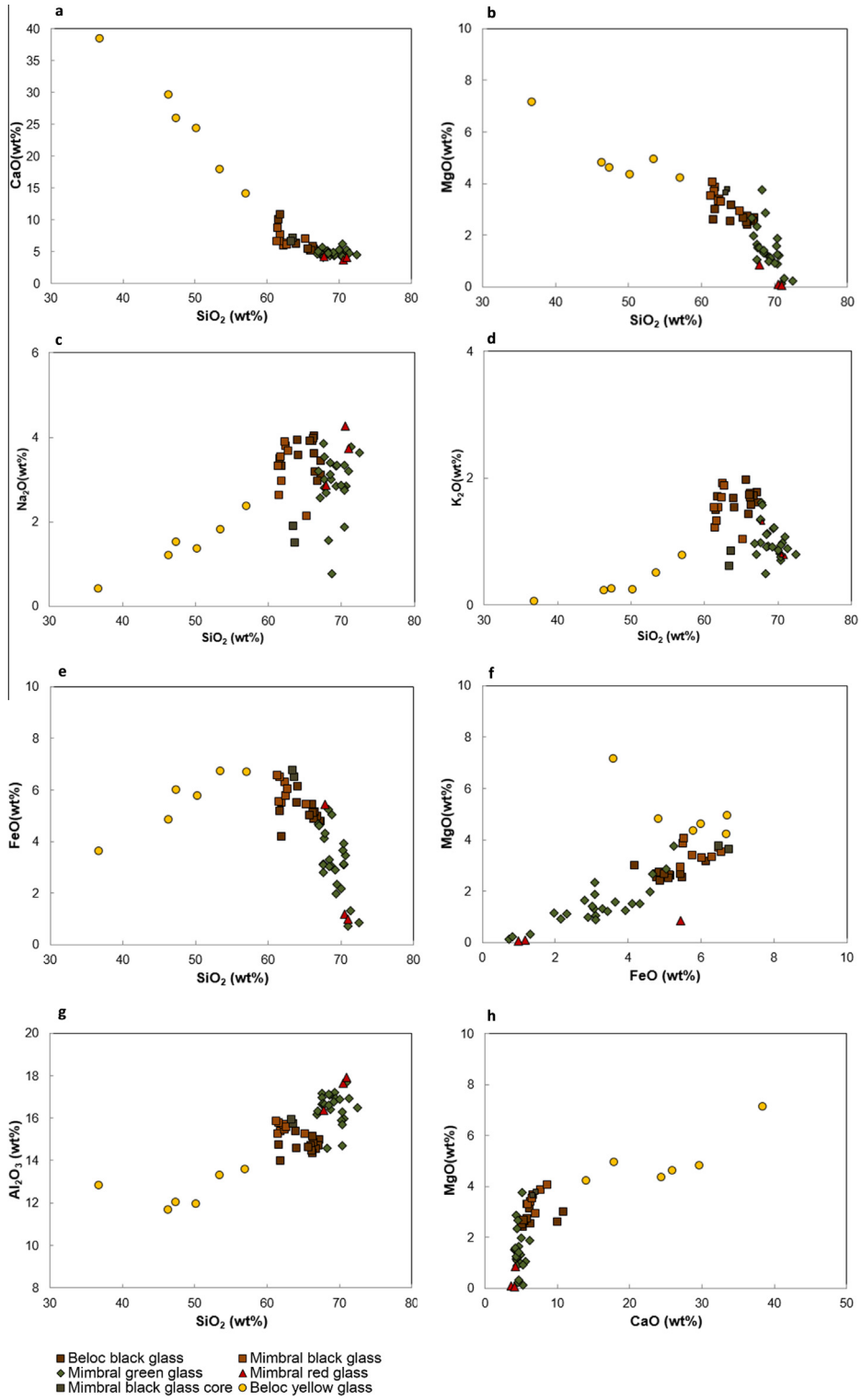

Fig. 13. Bivariate major element variation diagrams for all glass types. Major elements are determined with EMPA.

enriched in the HFSE, which are beyond the spatial resolution of the applied spot size (55–100 micron).

Due to large spot sizes, it was very difficult to obtain good quantitative spatially resolved information for the small L1 and L2 alteration layers, for which the thickness is at or below the resolution of the spot size. The mean compositions in Table 4 may represent contributions from both L2 and L1 layers. Still, some rare individual analyses on larger samples indicate that in the first ('palagonite') alteration phase, REEs are depleted by several orders of magnitude.

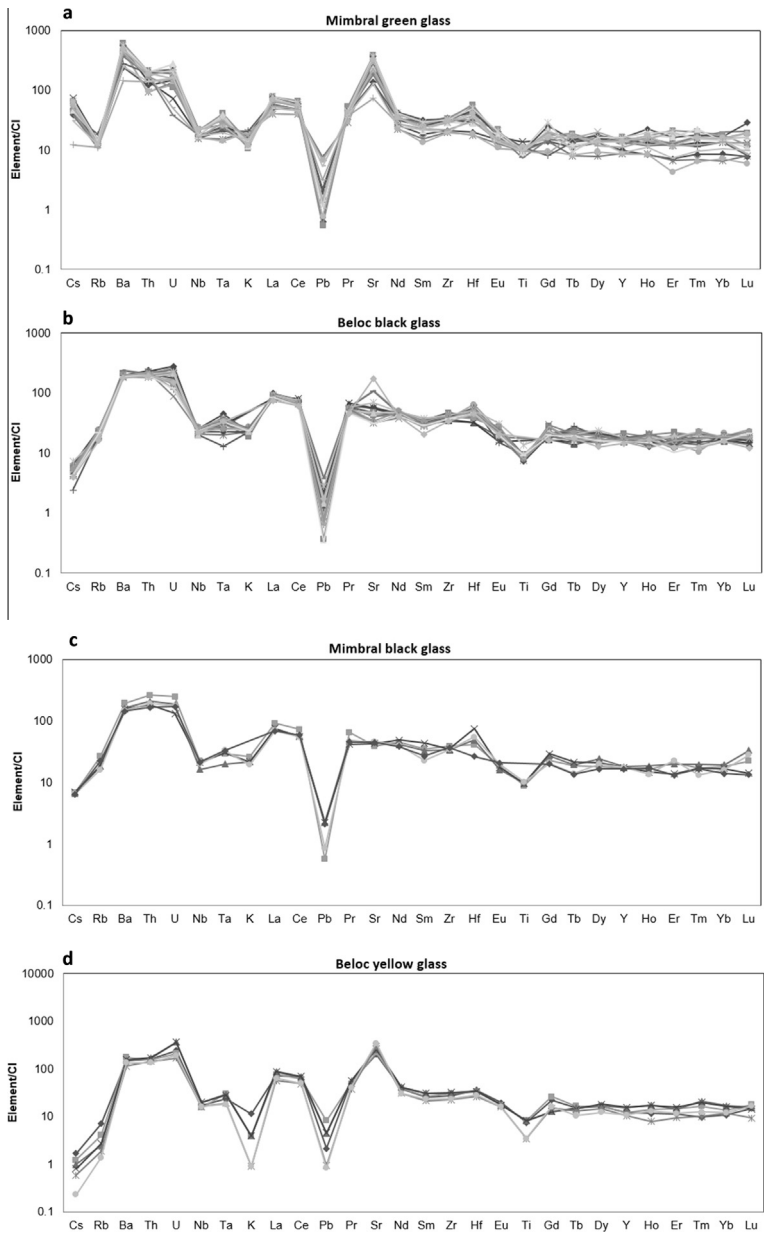

Fig. 14. CI-normalized spidergrams for single spot analyses from different glass groups determined by LA-ICP-MS. Glasses show a striking similarity for most trace elements. Yellow glass is enriched in Sr and Pb and depleted in Cs, Rb and K, indicating contribution from a marine carbonate/sulfate source. Green glasses are enriched in Sr, Ba and Cs compared to black glass suggesting sorption from seawater. CI normalization values from Lodders et al. (2009).

However, the CI-normalized patterns still resemble those of the adjacent glass phase, indicating that no significant internal fractionation occurred during the alteration process (Fig. 19a). In the second, well-crystallized smectite alteration phase, REE are mostly below LOD (sub ppm level) and almost completely lost to the hydrous solutions during the alteration process. This is consistent with observations from Staudigel and Hart (1983) who have shown that REEs become significantly depleted during glass alteration. In addition, the presence of a negative Ce anomaly (Fig. 19a), with Ce being one of the only two REE ions that are sensitive to the redox conditions of aqueous solutions (Zhong and Mucci, 1995), indicates relative large water-rock ratios during alteration at the Beloc locality. In some spherule rims, a positive instead of a negative Ce anomaly is observed (not shown). This may be the result of oxidative scavenging of Ce(IV) by precipitation into Fe oxyhydroxides (Otha and Kwave, 2001). At Mimbral, (Fig. 19b) the L1 layers show the same REE depletion without fractionation. In the chlorite/smectite alteration rim (L2), REE progressively become more depleted. Although REEs are incompatible elements and considered to be substantially insoluble in aqueous fluids, these elements can form soluble and mobile carbonate species (Ridley, 2012). In addition,

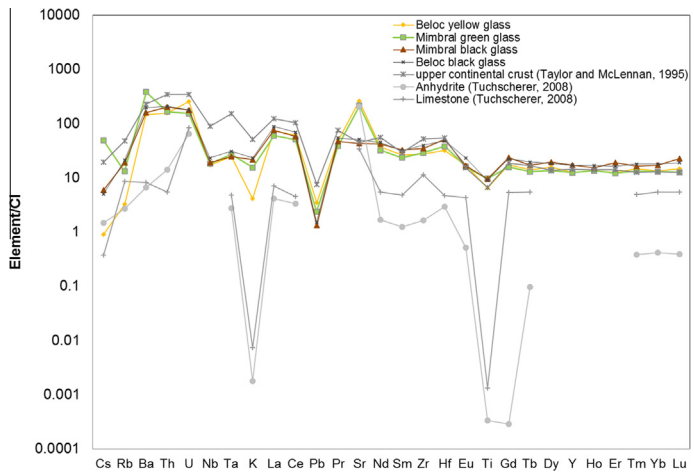

Fig. 15. CI-normalized spidergram for green, black and yellow glasses determined by LA-ICP-MS (mean values), average crustal continental crust (Taylor and Mclennan, 1995) and carbonate and anhydrite target rocks (Tuchscherer, 2008). Glasses are strikingly similar in composition. Yellow glasses show an enrichment of Pb, Sr and depletion in Cs, Rb and K. Green glasses are enriched in Cs, Ba, Pb and Sr. For the green glasses, the Pb, Cs, Ba and Sr enrichment most likely represents sorption from seawater fluids during hydration. For the yellow glass, Sr, U and Pb most likely represent a primary feature by admixture with marine carbonate/sulfate from the target. All values were normalized over CI values from Lodders et al. (2009). Typical values for continental crust from Taylor and McLennan (1995). (For interpretation of the references to color in this figure legend, the reader is referred to the web version of this article.)

Haskin et al. (1966) showed that calcite precipitation could effectively remove REEs from solution. Additional spot analyses carried out on the calcite matrices (Table 5) around spherules from Mimbral indicate that a significant portion of the REE budget (5–25%) is concentrated in the secondary calcite that is filling some of the spherules. This secondary calcite has a CI-normalized pattern that reflects the signature of microtektite glass, although the content is depleted by several orders of magnitude (Fig. 20a). When comparing whole rock analysis results from Arroyo El Mimbral with those for a batch including only the calcite-replaced spherules (Fig. 20b, Table 6), it becomes evident that most of the trace elements reside in the spherules, suggesting a close genetic relationship during alteration and emphasizing the buffering capacity of calcite cementation on the trace element signature of the deteriorating glass. At Beloc, there is a significant decrease in the REE content in the whole rock batch. Here, calcite replacement did not occur and the glass spherules are either completely replaced by smectite or host a relict glass core.

At Mimbral, K-rich fragments with perlitic fabrics show an almost complete loss of REEs (Table 4), the levels of which are below the LODs for the applied spot sizes (Table 4). However, average Zr/Hf and Nb/Ta ratios (Fig. 18b) resemble those for green, black, and yellow glasses, and still reflect the ratio of the original glass phase. In addition, K-rich shards show a distinct enrichment in Rb (Table 4). Their perlitic fabric, equivalent to that commonly found in hydrated high-silicic volcanic glasses, suggests that the K-rich fragments may be an alteration product of the felsic green glasses. This can also be deduced from Fig. 8H–J. Here, a relict green glass fragment with black glass core occurs in the center of a calcite-replaced spherule also hosting K-rich shards. The green glass is corroded at the edge. Two-dimensional energy dispersive element mappings (Fig. 21) show that this corrosion layer contains both Fe–Mg and K-rich alteration products. However, apart from the textural characteristics and immobile element ratios, the K-rich shards do not contain any geochemical information regarding the original melt composition.

4.4. 2-dimensional elements maps

Laser ablation-ICP-MS element distribution maps reveal important spatially resolved geochemical information beyond the capabilities of single spot measurements. Where sub-ppm concentration levels of most trace elements within the alteration phase are close to the LODs for spot sizes sufficiently small to obtain both quantitative and spatially resolved information, LA-ICP-MS element distribution mappings still produce qualitative estimations of the loss and gain of trace elements during the alteration process. Figs. 22–24 represent two-dimensional element distribution maps of spherules and glass fragments from both the Beloc and Arroyo El Mimbral localities, for selected major and trace elements. LA-ICP-MS mappings were compared with Energy Dispersive X-ray maps for major elements (Mg, Si, Al, Ti, Na, K) to validate the procedure. Fig. 22 shows part of a spherule from Beloc displaying a black glass core and surrounding double-layered alteration rim. EDS maps show that the glass becomes significantly depleted in Na, K, Si, Mg, and Ca in the first alteration layer (palagonite L1), while immobile Fe, Ti, and Al become relatively enriched. The second alteration layer (smectite L2) is characterized by a continued loss of Na, and an increase in Si, Mg, Ca, and K levels with respect to the L1 layer. Trace element distribution maps reveal that compared to the adjacent glass phase, Zr, Nb, Hf, Ta, Th, and Ni are enriched in the first alteration phase and parallel the behavior of Al, Fe, Ti, suggesting relative enrichment during early-stage

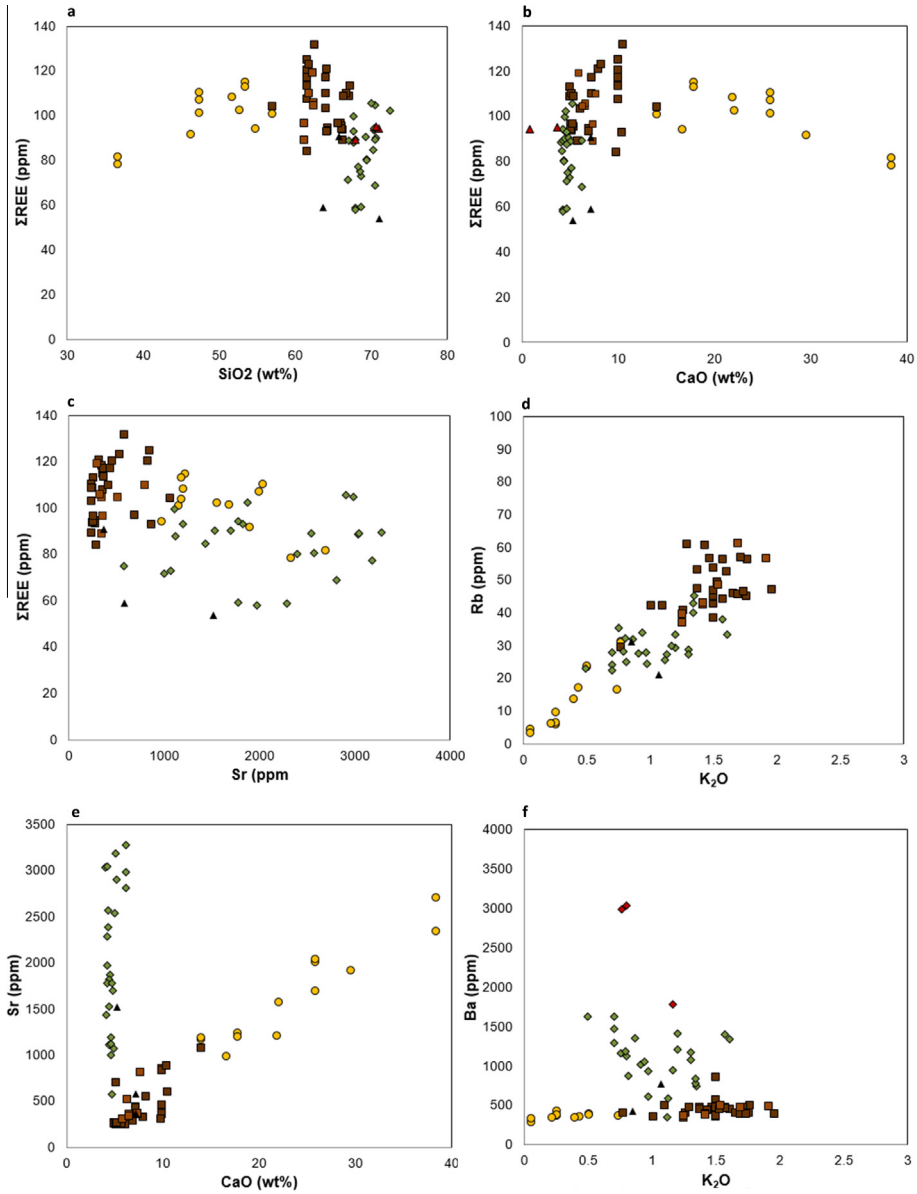

Fig. 16. Bivariate trace element variation diagrams for all glass types. Trace elements were measured with LA-ICP-MS applying a spot size of 55 and 100 μm.

palagonitization of the glass. In addition, element distribution maps visualize the presence of insoluble 'nuggets' of Fe–Ti rich phases hosting most of the immobile trace elements. These nuggets cannot be spatially resolved at the spot sizes used (55–100 μm), providing a plausible cause for scattered immobile element ratios amongst individual LA-ICP-MS spot analysis results. Compared to the L1 layer, Zr, Nb, Hf, Ta, and Th become slightly depleted in the second alteration phase L2. However, their absolute concentrations are similar to the original glass phase.

The REEs become progressively depleted in the first alteration phase, and their levels are mostly below detection limits in the second alteration phase, indicating almost complete loss to hydrous solutions during smectite crystallization. This is in agreement with LA-ICP-MS single spot drilling that indicates the same trend in REE depletion. LILE such as Rb, Ba, and Sr show a distinct behavior during the alteration process. Strontium and Rb become significantly depleted in the first alteration layer, but are slightly enriched in the second alteration layer. Barium progressively and strongly accumulates in the first and second alteration layers. Rubidium and Sr parallel the behavior of the major cations K and Ca released from the glass, while Ba is adsorbed from seawater. In addition, the Ba content is very high (~1500–2000 ppm), suggesting that Ba is efficiently adsorbed by the smectite clay.

In Fig. 23 a map for a spherule from Beloc is presented showing a black glass variety with patches of yellow glass, as can be seen in the lower right area of the glass. In addition, the spherule shows a bubble cavity that was filled with

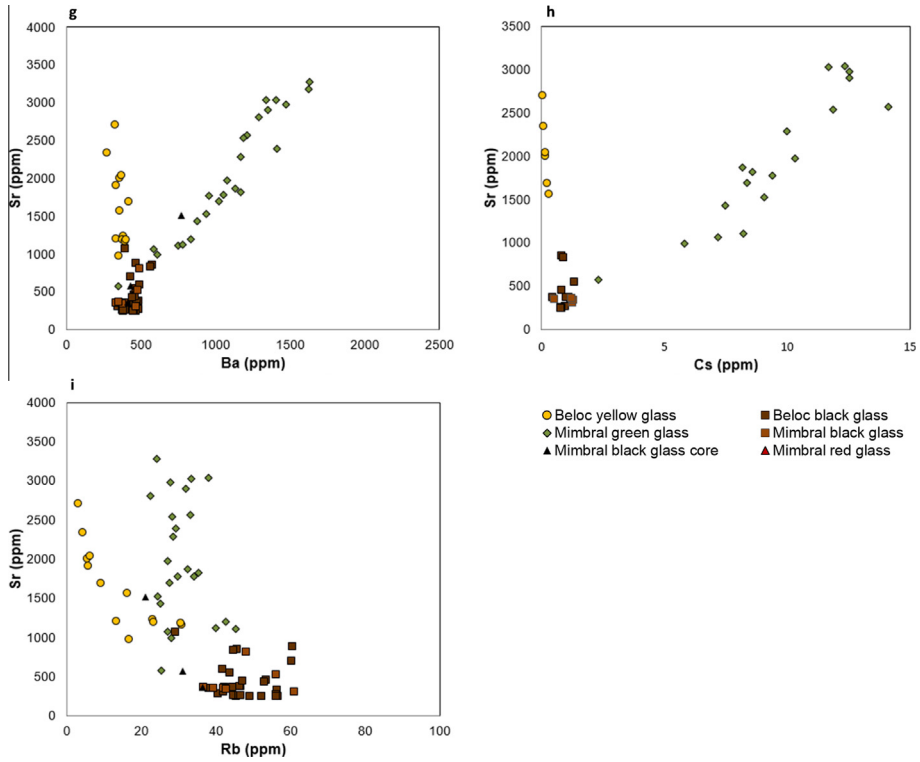

Fig 16. *(continued)*

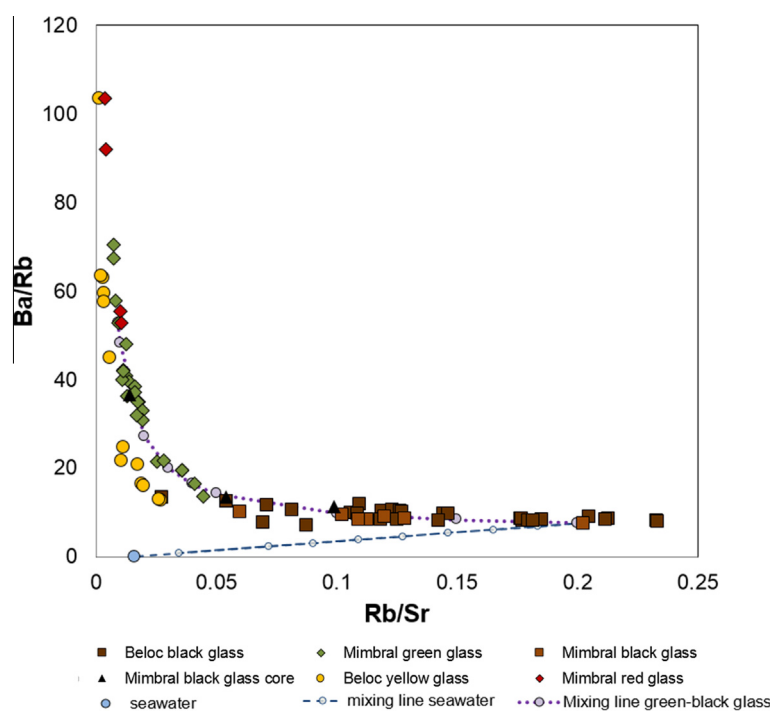

Fig. 17. Plot of Ba/Rb versus Rb/Sr for all glass types. Yellow and green glasses each define two different trends with black glass types (representing the melt-sheet end member), but converge at the high Ba/Rb, low Rb/Sr endmember. High Sr and low Rb and Ba contents are characteristic for a marine carbonate/sulfate source in the yellow glasses, producing high Ba/Rb, low Rb/Sr ratios. High Sr and Ba contents in the green glass suggest sorption from seawater during hydration. The green glasses show an opposite trend compared to simple addition of seawater, indicating preferred partitioning of alkalis during hydration. Seawater composition from GERM database (GERM- Geochemical Earth Reference Model). (For interpretation of the references to color in this figure legend, the reader is referred to the web version of this article.)

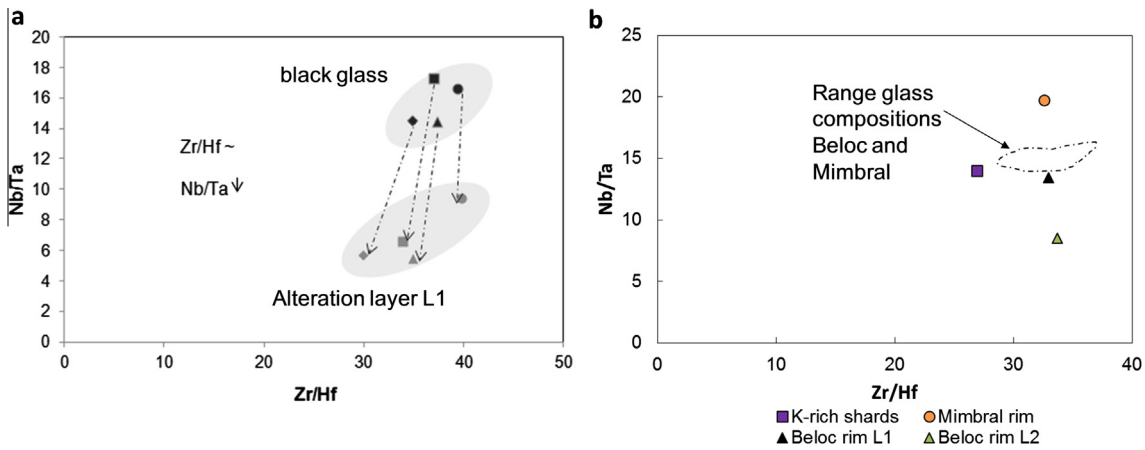

Fig. 18. (a) Plot of Nb/Ta versus Zr/Hf of selected individual glasses and their surrounding alteration layer (L1). The Nb/Ta ratio decreases significantly, while the Zr/Hf remains more or less the unaltered. (b) When the analyses for the various alteration phases (spherule rims at Beloc and Mimbral localities and K-rich, scalloped shards at Mimbral) are averaged, it becomes clear that the Zr/Hf and Nb/Ta ratios remain relatively unchanged during the alteration process. The large scatter amongst individual analyses most likely results from large spot analyses targeting 'nuggets' of immobile (Fe,Ti) phases that cannot be spatially resolved at the given spot size.

secondary material. Similar to the spherule mapped in Fig. 22, the first alteration layer shows a marked increase in immobile species such as Fe, Ti, Zr, Hf, Nb, and Th. REEs such as La, Ce, Pr, and Nd become depleted in the first alteration layer, and are mostly below the LODs in the second alteration phase. Strontium is concentrated in the yellow glass, along with Ca and Mg, but there is no clear variation in terms of other trace elements except for Rb that shows a small decrease. Although the bubble cavity was secondarily filled with similar smectite material, it does not show the enrichment in Zr, Hf, Nb, Ta, and Th, again emphasizing their immobile behavior and enrichment as a residual phase in the L1 and L2 layers.

Fig. 24 represents a green glass fragment with a black glass core. Two dimensional (EDS) distribution maps for selected major elements indicate that the green glass is enriched in Si, Al, Na, and K, and depleted in Mg, Ca, and Fe relative to the black glass core. LA-ICP-MS maps reveal an enrichment of Sr, Ba, and Cs in the green glass, consistent with single spot measurements carried out on selected glass chips. Although a 15 μm spot size limits spatial resolution in the fragment (300 μm wide), REEs such as Ce and La appear slightly depleted in the green glass compared to the black glass core.

4.5. Iron oxidation state

The measured iron oxidation state of six glasses selected from Beloc and Arrayo El Mimbral is reported in Table 7. Yellow glass exhibits a high $Fe^{3+}/\sum Fe$ ratio (0.65), while black glasses and black glass cores show a more variable iron oxidation state ($Fe^{3+}/\sum Fe$ of 0.55–0.77). Most striking are the (hydrated) green glasses, which have very low $Fe^{3+}/\sum Fe$ ratios (0.11–0.24). Red glasses with low iron contents have not been measured for their $Fe^{3+}/\sum Fe$ ratios due to low iron contents ($FeO_T < 2$ wt%). The results in Table 7 were compared with $Fe^{3+}/\sum Fe$ data on yellow and black glasses from Giuli et al. (2005) and Giuli et al. (2008) (Fig. 25) as determined with X-ray absorption near edge structure spectroscopy (XANES). The data set also includes the measurement of a single high Si, K glass (SiO_2 of 86%, see Koeberl and Sigurdsson, 1992). By plotting the $Fe^{3+}/\sum Fe$ versus the CaO content of the glasses (Fig. 25), Giuli et al. (2008) found a positive correlation, and attributed this to more oxidizing conditions in the melt resulting from the contribution of Ca-sulfate and Ca-carbonate comprising the target at the time of impact. Yellow and black glass from this study seems to confirm this interpretation. Interestingly, the green glasses have similar iron oxidation states as the high Si, K-type glass found by Koeberl and Sigurdsson (1992).

5. DISCUSSION

5.1. Glass alteration processes

Numerous authors have assessed the geochemical instability of natural and synthetic glasses in aqueous solutions and their subsequent alteration products (see Bunker, 1994, for an overview). It is a complex process that depends on both the intrinsic properties of the glass and the specific environmental conditions in which the alteration takes place (Utton et al., 2013). One of the primary factors is the composition of the glass. The alteration of low SiO_2 basaltic glass (sideromelane) is known to occur as a two-stage process involving initial hydration, followed by the formation of a palagonite precursor, which then crystallizes into a smectite type of clay (Morgenstein and Riley, 1974). High SiO_2 glass (obsidian-rhyolite) has been described as altering to perlite through simple hydration, followed by the crystallization of secondary clays. High Si–Al glasses tend to alter less rapidly because more H_2O is required to disrupt the highly polymerized Si–O and Al–O network (Scholze and Mulfinger, 1959). Compared to basaltic glass

Table 4
Trace element composition of alteration phases from Beloc (Haiti) and Arroyo El Mimbral locality (NE Mexico) as determined with LA-ICP-MS.

(μg/g)	Beloc rim L1 ('palagonite') Average ($n = 5$)	Beloc rim L2 ('smectite') Average ($n = 11$)	Mimbral spherule rim Average ($n = 8$)	Mimbral corrosion red tektite Average ($n = 1$)	Mimbral orange fragments Average ($n = 5$)	Mimbral K-rich 'shards' Average ($n = 5$)
Sc	28.0	22.1	18.1	18.3	13.7	19.4
V	28.0	87.6	329	139	61.3	218
Cr	59.2	36.2	98.3	70.1	96.9	102
Co	9.05	6.04	29.1	82.1	2.37	21.5
Ni	315	78.0	89.6	32.9	10.8	3.33
Cu	108	64.5	161	26.3	24.1	188
Zn	205	287	445	238	98.7	110
Ga	12.2	11.3	21.9	14.1	3.74	23.8
Ge	2.69	1.40	2.13	<LOD	3.60	<LOD
As	7.41	<LOD	68.5	<LOD	6.79	7.65
Rb	6.23	13.0	12.3	19.0	1.18	108
Sr	58.8	93.0	61.3	720	275	22.4
Y	2.82	2.75	2.86	4.67	8.14	1.82
Zr	206	144	46.3	102	154	44.0
Nb	8.44	4.03	14.1	2.37	8.92	3.00
Cs	<LOD	0.715	<LOD	5.10	<LOD	1.52
Ba	1539	1966	59.6	1537	383	61.9
La	1.71	1.95	0.63	1.46	2.90	0.28
Ce	5.20	3.74	1.85	3.75	17.2	1.44
Pr	0.75	0.54	0.32	0.59	1.11	0.16
Nd	2.57	2.08	1.10	2.11	5.39	0.55
Sm	0.83	0.56	<LOD	0.96	1.97	<LOD
Eu	<LOD	<LOD	<LOD	<LOD	0.49	<LOD
Gd	<LOD	<LOD	<LOD	<LOD	2.35	<LOD
Tb	0.30	<LOD	<LOD	<LOD	0.32	<LOD
Dy	0.80	0.60	0.74	0.96	1.67	0.34
Ho	0.41	<LOD	<LOD	0.38	0.43	<LOD
Er	0.57	0.34	0.96	0.89	1.12	<LOD
Tm	0.34	<LOD	<LOD	<LOD	<LOD	<LOD
Yb	0.80	0.40	0.71	0.95	1.54	<LOD
Lu	0.84	<LOD	<LOD	<LOD	<LOD	<LOD
Hf	6.25	4.27	1.42	2.94	5.33	1.64
Ta	0.63	0.47	0.72	0.31	0.59	0.21
W	<LOD	<LOD	2.33	<LOD	<LOD	<LOD
Ir	<LOD	<LOD	<LOD	<LOD	<LOD	<LOD
Pt	<LOD	<LOD	<LOD	<LOD	<LOD	<LOD
Au	<LOD	<LOD	<LOD	<LOD	<LOD	<LOD
Pb	12.7	5.23	88.2	1.53	117	6.17
Th	7.27	5.88	1.14	3.98	6.77	1.23
U	<LOD	<LOD	3.92	0.54	2.68	0.97

LOD, limit of detection.
n, number of analyses from which the average was calculated.

(sideromelane), alteration of highly silicic glass initially involves little solid-state change (Fisher and Schmincke, 1984), as the glass matrix takes up water (Friedman et al., 1966; Friedman and Long, 1976). Jezek and Noble (1978) noted that up to 3% water can be held in Si- and alkali-rich glass (obsidian) with low ion exchange across the entire compositional range of the glass, although Na_2O and K_2O can be particularly mobile (Friedman and Smith, 1958; Hunt and Hill, 1993).

Several geochemical, petrographic and textural characteristics suggest that K–Pg glassy spherules from both Beloc and Arroyo El Mimbral investigated in this study alter in a fashion similar to their volcanic counterparts. Bohor and Glass (1995) first proposed the hydration-palagonite model of rim formation for the K–Pg glassy spherules at Beloc. The present results show that at Beloc, relict black and yellow glasses with an average SiO_2 composition between 60–65 wt% (black) and 36–48 wt% (yellow) can be found in direct association with a double-layered alteration rim consisting of well-crystallized smectite ('L2') and poorly crystalline, partially isotropic palagonite-like material ('L1') directly at the glass interface. This poorly crystalline, Al-rich L1-layer represents a residual layer depleted in Na, K, Ca, Si, and Mg, and relatively enriched in immobile Al and Fe along with Zr, Hf, Nb, Ta, Th, Ti, and Ni.

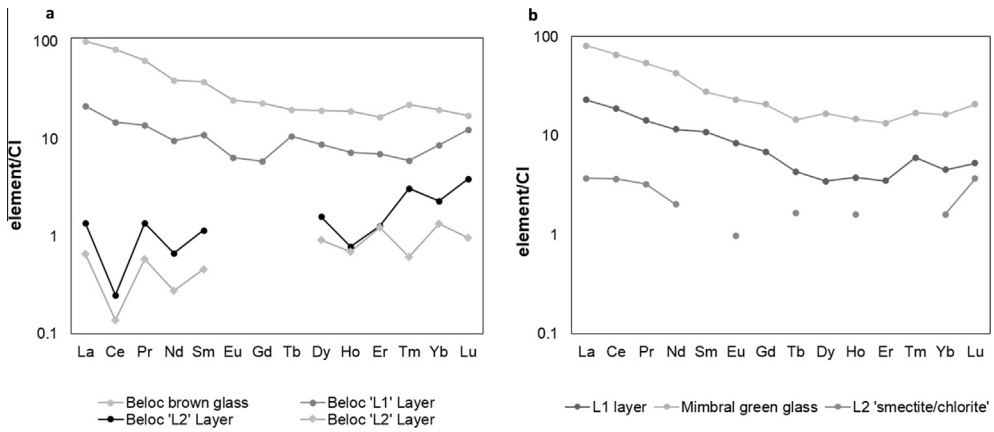

Fig. 19. (a) CI-normalized REE diagram for a selected microtektite spherule from Beloc. In the first alteration layer (L1), the REEs are depleted without internal fractionation. The smectite (L2) layer shows continued loss of REEs to solution with fractionation of the LREE from the HREE and a negative Ce anomaly. Eu, Gd, Tb are below the LOD. (b) Green glass chip from Mimbral with L1 alteration layer and chlorite/smectite rim. Sm, Gd, Dy, Er and Tm are below LOD. CI normalization values from Lodders et al. (2009).

Although most spherules at Arroyo El Mimbral have an alteration rim that shows textural characteristics similar to those from Beloc, the rims at Mimbral appear distinctly zoned. In addition, the smectite bands are articulated with finely dispersed Fe–Ti oxides. Morgenstein and Riley (1974) described the alteration of low SiO_2 glass (sideromelane) as a step-wise process with formation of successive palagonite/smectite bands: hydrolysis starts when water enters the glass structure and develops a hydration layer. Once a sufficient quantity of water is reached for crystallization, a smectite band will form. This process continues until all fresh glass is used up resulting in the formation of several, parallel smectite bands. In this context the prominent zonation of the smectite alteration rim at Mimbral may be attributed to changing fluid compositions and pH with time under closed-system conditions during palagonitization (Jercinovic et al., 1990), resulting in the formation of several palagonite/smectite bands with a slightly variable composition. Insoluble Fe- and Ti-oxides passively accumulate in the process and line the various palagonite/smectite bands, reminiscent of the former hydration fronts. At Beloc, this zonation has not or only barely been observed. In addition, two-dimensional EDS and LA-ICP-MS element mappings show that the smectite layer in Beloc glasses is in fact uniform both at the major and trace element level. Morgenstein and Riley (1974) suggested that the thickness of palagonite/smectite bands is likely related to the composition of the glass, with highly silicic glasses tending to have smaller banding widths. Moreover, Dohmen et al. (2013) suggest that lamellar alteration banding is an indication of spatio-temporal self-organization triggered by complex feedback mechanisms behind a propagating reaction front.

Despite being hydrated, green glasses found abundantly at Mimbral have normalized (100% water-free) major element compositions that are high in network formers SiO_2 and Al_2O_3, relatively high in alkalis Na_2O and K_2O, and low in the di-and trivalent metal oxides FeO, MgO, and CaO, which are network stabilizers. Even though the green glasses seem to form a highly polymerized glass network, these do not appear particularly resistant to aqueous alteration. Barkatt et al. (1984) noted that in addition to a high SiO_2 (and Al_2O_3) content, low alkali-contents compared to the di-and polyvalent metal oxide levels are required to sustain high corrosion-resistance in tektites. This is attributed to the fact that alkali ions are less strongly coordinated to the silicate network and have smaller hydration energies compared to the divalent alkaline earths Ca and Mg, making these the most mobile cations and the first to become involved in the ion-exchange process (Robinet et al., 2006). For the green glass, $Na_2O + K_2O/MgO + FeO + CaO$ ratios are relatively low (<1). This may probably result from an underestimated alkali content due to the onset of ion-exchange.

Although a detailed study of the structural properties of the glasses and alteration phases using Raman spectroscopy is beyond the scope of this paper, important information regarding structural changes associated with the alteration process may be derived from the Raman spectra. A typical spectrum of a (pristine) silicate glass is characterized by the presence of two broad bands originating from the bending ($\sim$500 cm^{-1}) and stretching ($\sim$800–1200 cm^{-1}) vibrations of SiO_4-tetrahedra in a three-dimensional network (Baert et al., 2011). The presence (or absence) of modifier cations (Na, K, Ca, Mg, Fe, etc.) in various proportions within the glass changes the relative intensities, shape, and position of the peaks of these two main vibration modes (Colomban et al., 2006). Consequently, interpretation of the structural composition of glass using Raman spectroscopy is based on the Q_n model, in which Q_n represents the different tetrahedral species in the glass network with n the number of bridging oxygens: Q_0 ($\sim$800–850 cm^{-1}) represents an isolated tetrahedron, whereas Q_1 ($\sim$900–950 cm^{-1}), Q_2 (950–1000 cm^{-1}) and Q_3 (1050–1100 cm^{-1}) tetrahedra share 1, 2, and 3 oxygens, respectively. Q_4 is fully polymerized as in pure SiO_2 ($\sim$1150–1250 cm^{-1}) (Baert et al., 2012). Compared to non-hydrated black and yellow glasses, the green hydrated glasses show a prominent decrease of the intense peak in the high frequency region around 1100 cm^{-1}

Table 5
Trace element compositions for diagenetic calcite in Mimbral spherules as determined with LA-ICP-MS.

(μg/g)	MIMBR Cc 1	MIMBR Cc 2	MIMBR Cc 3
Sc	2.13	5.83	0.76
V	<LOD	<LOD	0.52
Cr	2.02	10.4	1.68
Co	20.2	<LOD	<LOD
Ni	8.82	<LOD	<LOD
Cu	1.38	<LOD	<LOD
Zn	<LOD	<LOD	1.85
Ga	<LOD	<LOD	<LOD
Ge	<LOD	<LOD	<LOD
As	<LOD	<LOD	<LOD
Rb	<LOD	<LOD	<LOD
Sr	163	203	129
Y	1.87	6.62	2.80
Zr	<LOD	<LOD	<LOD
Nb	<LOD	<LOD	<LOD
Cs	<LOD	<LOD	<LOD
Ba	<LOD	<LOD	<LOD
La	1.16	4.91	1.24
Ce	1.93	7.92	1.84
Pr	0.24	0.87	0.26
Nd	1.05	3.40	1.07
Sm	0.28	0.93	0.28
Eu	0.08	0.27	0.10
Gd	0.36	0.99	0.39
Tb	0.05	0.18	0.06
Dy	0.36	1.05	0.39
Ho	0.10	0.28	0.09
Er	0.36	0.94	0.36
Tm	0.04	0.12	0.06
Yb	0.30	0.82	0.35
Lu	0.05	0.12	0.05
Hf	<LOD	<LOD	<LOD
Ta	<LOD	<LOD	<LOD
W	<LOD	<LOD	<LOD
Ir	<LOD	<LOD	<LOD
Pt	<LOD	<LOD	<LOD
Au	<LOD	<LOD	<LOD
Pb	6.49	0.17	0.23
Th	0.13	1.20	0.263
U	0.11	0.07	1.10

MIMBR Cc 1, MIMBR Cc 2, MIMBR Cc 3 represent individual spot analyses on calcite filling inside the spherules.
LOD, limit of detection.

(Fig. 11). As this peak is associated with the symmetric Si–O stretching vibrations of the Q_3 species (Na^+, K^+), Robinet et al. (2008) attributed its disappearance to the leaching of the alkalis out of the glass causing the gradual loss of the depolymerized structure coordinated to alkali cations ($Q_3 \sim 1000\ cm^{-1}$). This may indicate that the ion-exchange reaction leaches alkalis (Na and K) out of the structure but leaves divalent and trivalent stabilizer cations, such as Ca, Mg, and Fe largely undisturbed (Robinet et al., 2008). The Raman spectrum of the red glass does not correspond to a typical glass structure. The vibrational bands in the 800–1200 cm^{-1} stretching region are significantly decreased, and the overall spectrum resembles that of vitreous silica, indicating increased polymerization. In addition, the OH peak is not as prominent as can be seen in the green glass variety. The red glass probably represents a more advanced stage in the alteration of the green glass type, indicating breakdown and restructuring of the silicate network.

The Raman spectra of the green hydrated silica glasses display a peak in the high-wave number region (3100–3750 cm^{-1}), assigned to stretching vibrations of H_2O molecules and OH groups. However, it is important to evaluate the speciation of water in the glass structure, to assess the extent to which ion exchange reactions have occurred. Water can diffuse into the glass structure either through diffusion of the molecular species H_2O through void spaces between oxygen atoms in the structure (Mazer et al., 1991; Bunker, 1994; Robinet et al., 2006), or dissociate causing an ion exchange process in which the alkali cations (Na^+, K^+) are replaced by H^+ or H_3O^+ to preserve electroneutrality. In the latter case, alkalis are leached out of the silicate network as water reacts with the silicate network to form silanols (Si–OH). According to Bunker (1994), these silanols may react with each other, resulting in the formation of new Si–O–Si species (and molecular water) and a higher degree of polymerization. Green glasses exhibit a sharp increase in the intensity of the band around 500 cm^{-1} (Fig. 11). This band is associated with Si–O–Si bending vibrations and can be attributed to the formation of new Si–O–Si species (Robinet et al., 2006). In addition, the broad band in the 3100–3750 cm^{-1} region contains components associated with OH in molecular water (3000–3550 cm^{-1}) and hydroxyl groups, such as silanols (3450–3700 cm^{-1}). This indicates that both species are present in the green glasses. Consequently, the green glasses can be considered to represent the first step in the hydration of highly silicic glasses. The delivery of free H^+ and H_3O^+ in the surrounding acidic (low pH) solutions triggers ion exchange with the most mobile cations (alkali) from the glass structure (Bunker, 1994):

$$\equiv Si{-}O{-}Na^+ + H^+ \rightarrow \equiv Si{-}OH + Na^+$$

$$\equiv Si{-}O{-}Na^+ + H_3O^+ \rightarrow \equiv Si{-}OH + Na^+ + H_2O$$

Although the network remains largely undisturbed, some rearrangements may occur by the reaction between the silanols, as these polymerize forming new Si–O–Si bonds.

$$\equiv Si{-}OH + HO{-}Si\equiv \rightarrow \equiv Si{-}O{-}Si\equiv + H_2O$$

Further hydrolysis within the hydrated layer may result in restructuring to form crystalline phases (chlorite), or at the surface of the glass hydrolysis can result in etching or complete dissolution of the glass structure (Mazer et al., 1991).

Apart from glass composition, the importance of fluid chemistry becomes evident from textural constraints in particular spherules. At Arroyo El Mimbral, locally, the lack of a thick, Fe–Mg alteration rim and dominant occurrence of 'hollow' spherules filled with secondary calcite indicates that most of the glass has simply dissolved. Calcite cementation attests to high pH and alkaline conditions, as a high pH lowers the solubility of calcium carbonate thus promoting precipitation. In this context, the corrosion mechanism

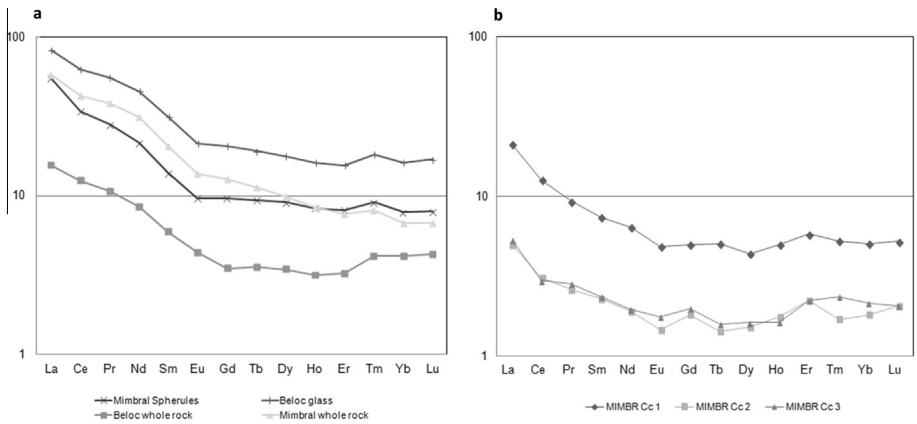

Fig. 20. (a) CI-normalized REE diagram and spidergram for selected whole-rock batches in Arroyo El Mimbral and Beloc (solution ICP-MS following acid-digestion). (b) CI-normalized REE diagram for selected spots on the calcite matrix in spherules from Mimbral (using LA-ICP-MS and a 100 μm spot size). At Mimbral, the secondary calcite seems to buffer the REEs (and a large amount of other trace elements) during the alteration process, suggesting a close genetic and temporal relation. At Beloc, where spherules are altered to smectite and often host a glass core, the REEs are significantly depleted in the whole rock batch.

Table 6
Trace element data for Mimbral and Beloc spherules, glasses and whole rock using ICP-MS following acid digestion.

(μg/g)	MWR Mimbral whole rock	MSp Mimbral spherules	BWR Beloc whole rock	BGL Beloc glass
Sc	7.45	7.87	12.09	18.0
Ti	2113	2509	2920	3998
V	66.0	47.1	59.3	105
Cr	27.0	27.2	18.2	22.9
Co	15.8	20.8	13.8	13.6
Ni	29.5	35.8	66.0	16.2
Cu	76.9	50.3	20.8	27.8
Zn	32.9	19.3	34.0	36.5
Ga	6.41	3.76	5.86	10.56
Rb	21.9	13.1	5.03	41.8
Sr	526	480	102	382
Y	14.9	15.3	4.47	26.6
Zr	50.8	44.6	83.7	116
Nb	3.02	3.78	4.05	4.66
Sn	0.36	0.26	0.42	0.45
Sb	0.76	0.63	0.23	0.42
Cs	0.85	0.56	0.30	1.08
Ba	75.1	66.0	499	484
La	13.3	12.7	3.61	19.2
Ce	26.4	21.2	7.71	39.0
Pr	3.54	2.61	0.99	5.14
Nd	14.3	9.87	3.90	20.8
Sm	2.97	2.02	0.86	4.54
Eu	0.75	0.53	0.24	1.17
Gd	2.54	1.92	0.69	4.05
Tb	0.40	0.34	0.13	0.68
Dy	2.35	2.16	0.82	4.24
Ho	0.47	0.47	0.18	0.91
Er	1.24	1.31	0.53	2.53
Tm	0.19	0.22	0.10	0.43
Yb	1.10	1.28	0.68	2.64
Lu	0.16	0.19	0.10	0.40
Hf	1.37	1.13	2.32	3.22
Ta	0.23	0.30	0.11	0.16
Pb	5.93	7.78	2.49	5.33
Th	2.27	2.20	2.83	5.64
U	2.22	2.64	0.21	1.20

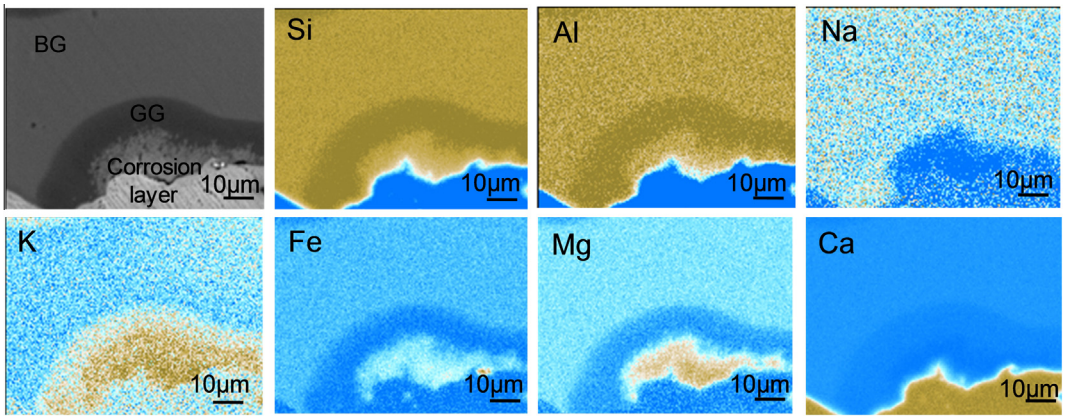

Fig. 21. False color 2-dimensional Energy dispersive X-ray element mappings from a relict green glass (GG) piece with black glass (BG) core in the center of a calcite-replaced spherule (see also Fig. 11H–J) from the Arroyo El Mimbral locality. Color index (blue to brown) represents minimum and maximum count rates. The green glass is corroded at the edge showing both K, Mg and Fe-rich alteration products. (For interpretation of the references to color in this figure legend, the reader is referred to the web version of this article.)

of the glass can more easily be understood in terms of fluid chemistry. In alkaline solutions at high pH (>9), hydrolysis and simple dissolution of the glass network seems to dominate over the ion exchange process, because OH^- species will catalyze a nucleophilic attack on the Si–O–Si sites at the interface between the glass and the solution (Doremus, 1994; Robinet et al., 2006), as indicated by the reaction:

$$\equiv Si{-}O{-}Si\equiv + OH^- \rightarrow \equiv Si{-}O^- + HO{-}Si\equiv$$

$$\equiv SiO^- + H_2O \rightarrow \equiv Si{-}OH + OH^-$$

Consequently, under alkaline conditions, dominating in the calcite-replaced spherules at Arroyo El Mimbral, the glass network will simply dissolve without build-up of insoluble reaction products at the surface. In addition, calcite cementation will have a buffering effect on the dissolution of the glass. This is consistent with a recent study by Utton et al. (2013), who emphasize that calcium plays an important role in the long-term durability of nuclear waste glasses at high pH through the formation of calcium precipitates on the reaction surface. This also explains the dominant occurrence of relic green glass in the center of calcite-replaced spherules. In addition, the observed variable composition in the spherule rims ranging between smectite and chlorite is consistent with the presence of mixed green (high Si) and black (low Si) glasses producing different reaction products.

Green glass with low analytical totals has previously been reported by Bohor and Betterton (1993) and Claeys et al. (1993). Hildebrand et al. (1993) noted the presence of strongly, but variably enriched Sr, Cs, and Ba concentrations in whole rock analyses from the green glass variety. Oddly, detailed petrographic descriptions and geochemical data have never been reported. Remarkably, Smit et al. (1992b) designate the green glass variety as K-rich. In this context it must be noted that Koeberl and Sigurdsson (1992) also report the presence of one pristine high Si, K-glass fragment at the Beloc locality. An interesting observation is that the $Fe^{3+}/(Fe^{2+} + Fe^{3+})$ ratio of this high Si, K-variety (Fig. 25) is remarkably similar to the $Fe^{3+}/(Fe^{2+} + Fe^{3+})$ for green glasses at Mimbral (this study). In addition, Alvarez et al. (1992b) report data for high Si, K glasses at DSDP sites 540 and 536 (Fig. 1A) with compositions similar to green glasses from Mimbral reported in this study and that from Smit et al. (1992b). The compositional variation of the green glasses as compared to literature data is given in Table 8. Note that in all (pristine) green glasses reported in literature, Si, Ca and alkali content seem to vary to a large extent, while Al content remains consistently high, suggesting admixture (or exsolution) of mineral melts composed of $CaAl_2Si_2O_8$, $NaAlSi_3O_8$, $KAlSi_3O_8$ and SiO_2 in various proportions with the homogenized melt sheet as represented by the black glass variety. Interestingly, one glass fragment from Alvarez et al. (1992b) has a pure K-feldspar composition (Table 8). From this, we may speculate that the green, high K-variety reported by Smit et al. (1992b) and Koeberl and Sigurdsson (1992) may in fact represent the high Si, Al, K compositional end member for the green glasses investigated in this study. If so, this provides additional support to the interpretation that the green, hydrated glasses with low analytical totals initially represented high Si, (Al), K-glasses that underwent ion-exchange in which alkalis may have been leached out of the glass structure.

The co-occurrence of both relict green glass and K-rich hydrated glass fragments with a perlitic fabric (Fig. 8A–D) as observed in this study suggests that under specific conditions, the green, high SiO_2-glass may alter to perlite in a fashion similar to the high-SiO_2 volcanic glass rhyolite/obsidian. This is an interesting observation, because it implies that although geochemical data may have been lost, the textural characteristics of the alteration phase still relate to the precursor. Several studies on naturally hydrated obsidian indicate depletion of Na_2O with associated enrichment in K_2O in perlite compared to the adjacent glass (Noh and Boles, 1989; Conde and Ihinger, 2011). On a $Na_2O + CaO$ versus $K_2O + MgO$ plot (Fig. 26), the green glasses define a trend with a slope similar to the K-rich fragments, indicating a genetic relationship dominated by Na and Ca exchange with K and Mg. This genetic relationship

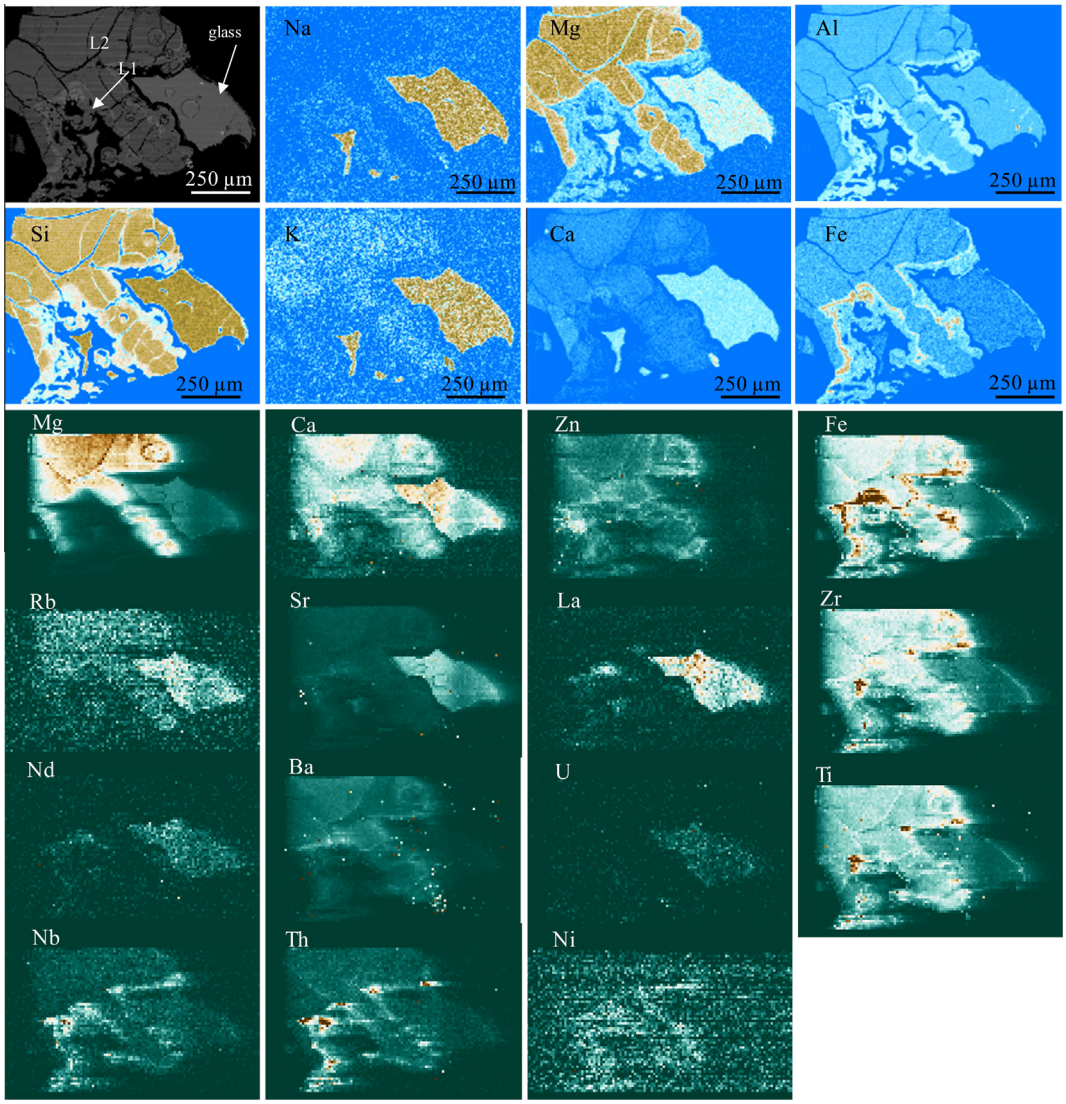

Fig. 22. Two-dimensional element distribution maps for major elements Na, K, Mg, Si, K, Ca, Fe, Al and Ti based on EDS spectra for a glass spherule from the Beloc locality. 2D element distribution maps for selected major and trace elements obtained using LA-ICP-MS. The color index indicates relative element concentrations based on minimum and maximum count rates. Strontium, Rb, U and REEs such as La become progressively depleted in the first and second alteration layer. However, Ba becomes enriched in the process. Ti and Fe are passively accumulated along the hydration fronts. Ni and immobile HFSE such as Zr, Nb and Th appear to follow the behavior of Fe and Ti. (For interpretation of the references to color in this figure legend, the reader is referred to the web version of this article.)

between the green glass and the K-rich fragments suggests that the green glasses may alter into different reaction products, depending on environmental conditions. Consequently, in the calcite-replaced spherules that host the K-rich, scalloped fragments, rapid glass dissolution and calcite precipitation may have resulted in a decreased pH and an overall changing fluid composition, exerting a negative feedback reaction on the alteration mechanism affecting the remaining glass fragments.

The co-occurrence of small, hydrated green glass fragments in calcite-replaced spherules, along with an Fe–Mg chlorite alteration rim and the formation of perlite-like K-rich alteration products suggests that the alteration of high SiO_2 glass involves numerous competing reaction processes (Mazer et al., 1991), including both molecular water diffusion, ion exchange, surface reaction (etching/dissolution), and secondary mineral precipitation (Dran et al., 1988; Abrajano et al., 1989; Petit et al., 1990). These processes are controlled by complex feedback mechanisms between glass composition and the characteristics of the surrounding fluids (Gislason and Eugster, 1987; Gislason et al., 1993; Steefel and Lasaga, 1994; Stumm and Morgan, 1996; Stroncik and Schmincke, 2002). A nice example of this genetic relationship is illustrated in Figs. 8H–J and 21, in which a green glass fragment, an Fe(Mg) alteration rim and K-rich shards can all be observed in one single spherule. The green glass fragment (Fig. 21) is located in the left part of a calcite-replaced spherule (Fig. 8H–J) containing numerous small K-rich shards and a thin Fe(Mg) alteration rim. In the early stage of

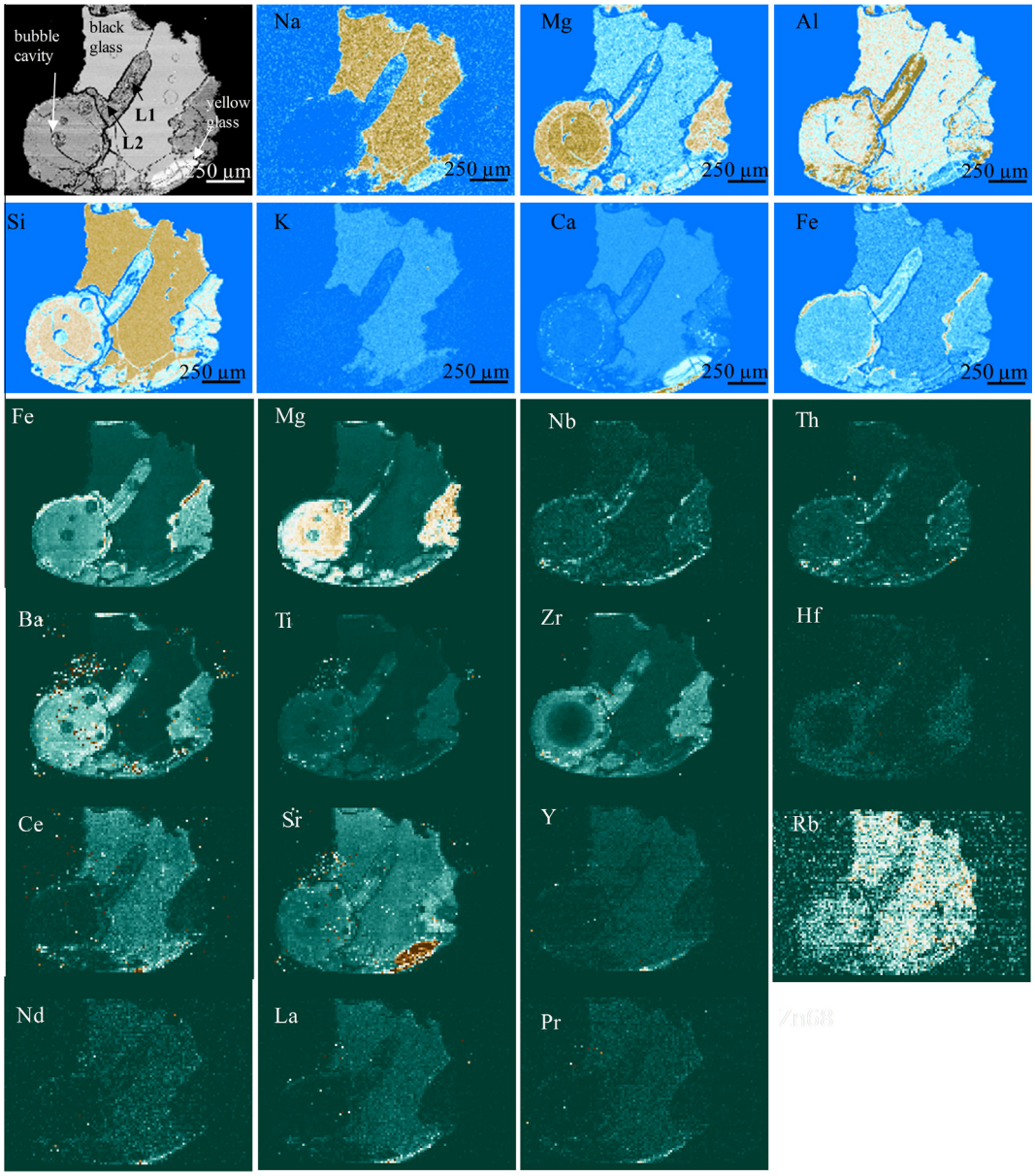

Fig. 23. Two-dimensional EDS and LA-ICP-MS element distribution maps for major and trace elements for a spherule from the Beloc locality. Zirconium, Nb, Th and Hf follow Fe and Ti and passively accumulate in the process. REEs gradually become depleted in the first alteration layer but are almost completely lost to solution in the second alteration phase (smectite). The yellow glass shows a marked enrichment in Sr. Note the bubble cavity that is filled with secondary material. (For interpretation of the references to color in this figure legend, the reader is referred to the web version of this article.)

the alteration process, rapid hydration and ion-exchange of the green glass resulted in the precipitation of secondary phases, forming a thin Fe(Mg) alteration layer now constituting the spherule rim. Due to high pH conditions, the rate of glass dissolution was higher than the rate of ion-exchange. The glass rapidly dissolved and calcite precipitated. Transformation of the hydrated, green glass fragments into K-rich alteration products most likely occurred in the latest stage of the alteration process, when most of the glass had already dissolved and calcite precipitation had cemented large parts of the spherule's interior. As a result, overall porosity was reduced, restricting the seawater circulation and gradually closing the system. In some places, rapid calcite cementation stalled the alteration process entirely before transformation into a K-rich alteration product, and a relict, hydrated green glass fragment was preserved.

5.2. Implications for cratering dynamics and target rock composition

Although green glasses seem to have experienced significant ion exchange of the alkalis Na and K during hydration and minor sorption of Sr, Ba, and Cs from

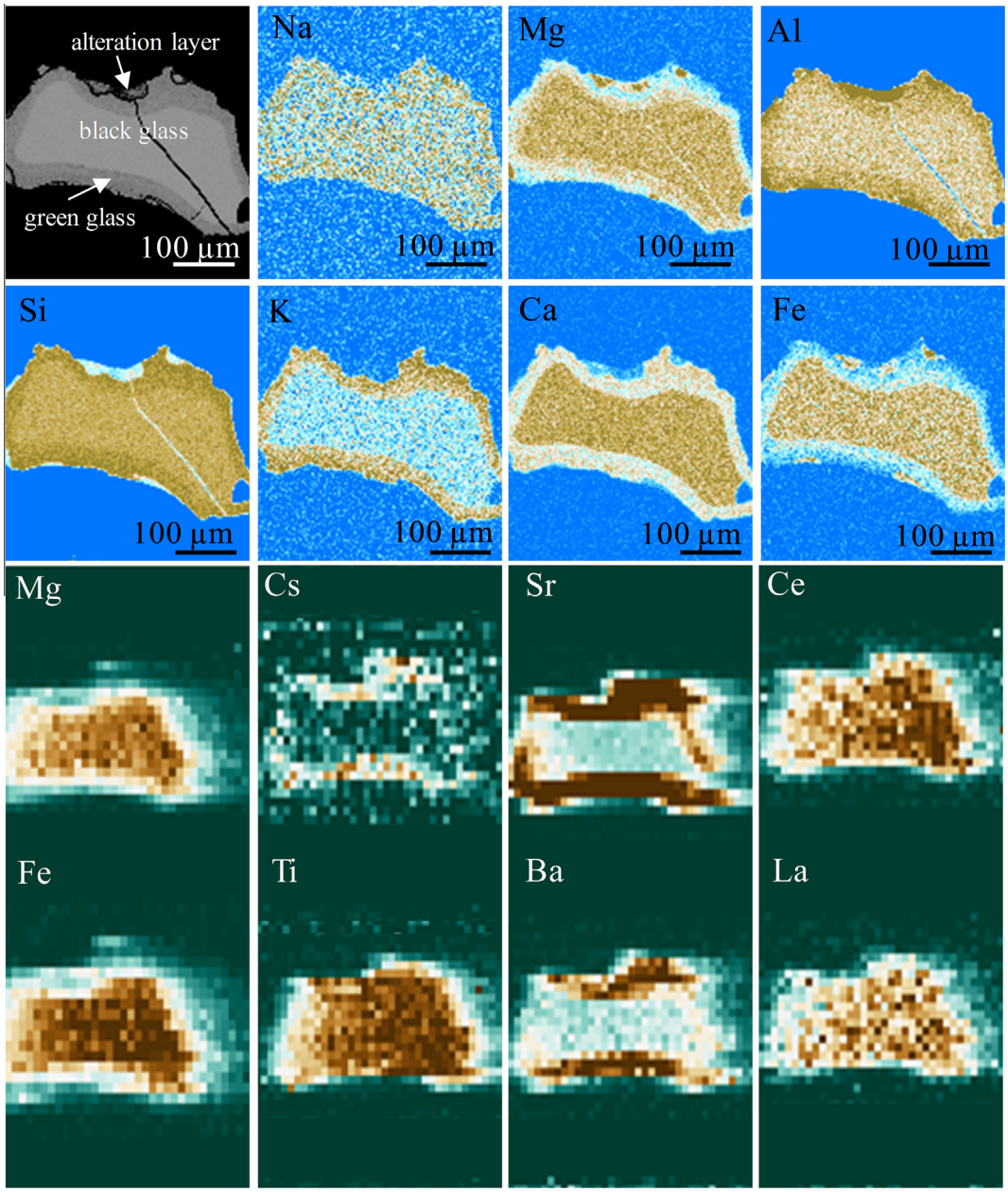

Fig. 24. EDS and LA-ICP-MS element distribution maps for selected glass fragments from Arroyo El Mimbral, showing a high SiO_2 green glass with a black low SiO_2 core. The green glass is enriched in Sr, Ba and Cs and depleted in Fe, Ti, Mg and Ca. (For interpretation of the references to color in this figure legend, the reader is referred to the web version of this article.)

surrounding fluids, pristine trace element signatures (REEs, HFSEs) indicate that the glass composition is still largely representative for the original melt composition. Although the Si, Al, Na, and K contents may initially have been higher, the generally high SiO_2, Al_2O_3, Na_2O and K_2O as well as low MgO, FeO, and CaO levels are indicative of a more felsic melt precursor for the green glass type. This is in strong contrast to earlier studies on glass spherules at proximal K–Pg sections in northeastern Mexico. Kettrup and Deutsch (2003) emphasize the presence of a substantial mafic to intermediate component amongst the target lithologies based on Rb–Sr and Sm–Nd model ages of (altered) chlorite spherules at La Lajilla (Fig. 1). Schulte et al. (2003) propose a mafic precursor for the (altered) Fe–Mg rich glass spherules at the La Sierrita locality (Fig. 1).

The absence of the green glass variety at the Beloc locality might be the result of a preservation effect, in which the combination of a highly siliceous composition, high alkali content and high pH conditions causes this glass type to undergo simple dissolution rather than palagonitization/clay mineral formation. However, since at Beloc no hollow or calcite-filled spherules were found throughout this work, we also consider the possibility that the green glass might in fact represent a variety that was originally less distributed

Table 7
$Fe^{3+}/\sum Fe$ for selected glass types determined with EMPA.

	2MIMBR1 Mimbral green glass	2MIMBR2 Mimbral green glass	2MIMBR Mimbral brown core	2MIMBR Mimbral brown glass	BLC1 Beloc brown glass	BLC2 Beloc yellow glass
$Fe^{3+}/\sum Fe$	**0.11**	**0.24**	**0.65**	**0.55**	**0.77**	**0.65**
±	0.08	0.10	0.06	0.06	0.05	0.05
Wt% oxide						
Na_2O	2.82	2.80	2.06	3.06	3.73	1.45
MgO	1.03	1.02	3.36	3.33	2.37	4.20
SiO_2	59.7	62.0	57.2	59.5	64.8	47.8
Al_2O_3	14.9	14.1	14.0	15.3	15.4	11.7
K_2O	1.16	0.81	0.85	1.41	1.74	0.40
CaO	3.63	3.70	7.80	6.38	5.61	26.7
TiO_2	0.66	0.59	0.65	0.75	0.62	0.55
MnO	0.09	0.06	0.10	0.11	0.12	0.12
FeOT	3.02	2.27	5.03	6.04	5.12	4.91
P_2O_5	0.16	<LOD	0.13	0.18	0.11	0.14
SO_2	<LOD	<LOD	<LOD	<LOD	<LOD	0.87
Total	87.2	87.5	91.5	96.1	99.7	98.9

'Bold' values in Table 7 are highlighted specifically just to emphasize the Fe^{3+}/FeT ratios in the table.

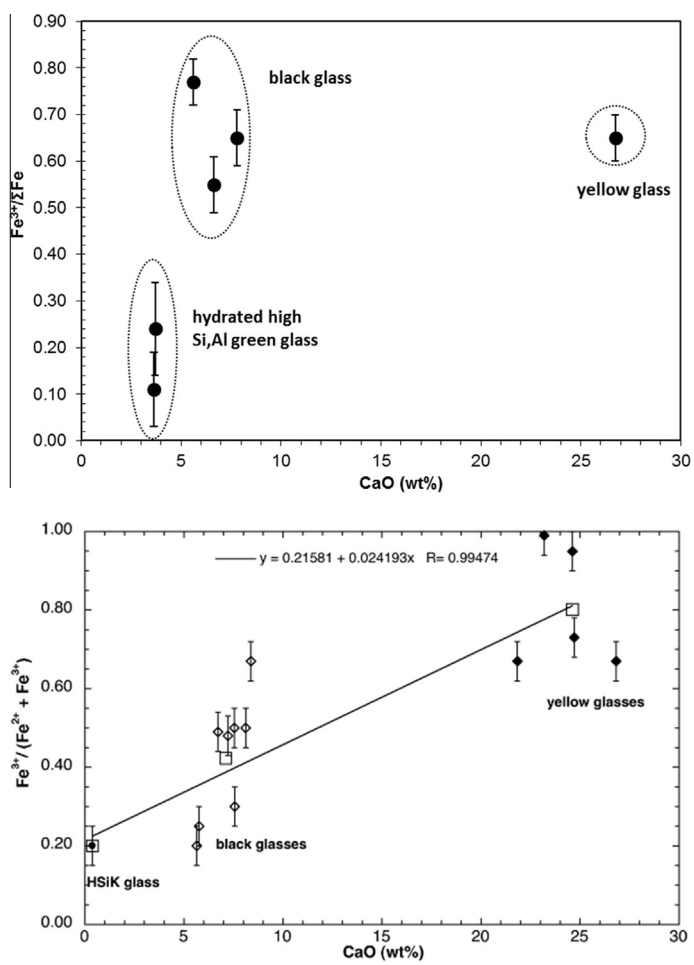

Fig. 25. Plot of the $Fe^{3+}/\sum Fe$ versus CaO content of selected microtektite glasses from Chicxulub at the Mimbral and Beloc localities. (A) This study, as determined via EPMA by measuring the self-absorption induced shift of the Fe Lα-peak. (B) From Giuli et al. (2008), as measured with Fe K-edge XANES spectroscopy.

Table 8
Compositional variation of black, green and yellow glasses at Beloc and Arroyo El Mimbral localities compared to literature data.

Beloc				Arroyo El Mimbral						DSDP 540 and DSDP 536				
	Black glass°, this study	Yellow glass°, this study	High Si,K glass°, Koeberl and Sigurdsson (1992)	Green glass°, Smit et al. (1992b)	Green glass*, Bohor and Betterton (1993)		Green glass*, this study		Black glass°, this study		Color not specified°, Alvarez et al. (1992b)	Color not specified°, Alvarez et al. (1992b)	Color not specified°, Alvarez et al. (1992b)	Color not specified°, Alvarez et al. (1992b)
					Average	Recalc	Average	Recalc.						
SiO_2	64.2	47.9	66.32	66.20	60.82	67.3	59.3	67.1	61.3	SiO_2	70.4	68.49	62.67	60.4
Al_2O_3	14.4	12.4	19.65	18.73	14.88	16.47	14.4	16.2	15.3	Al_2O_3	20.95	19.32	21.58	20.87
FeO	5.15	5.54	5.3	5.67	4.35	4.82	4.35	4.92	6.06	FeOT	0.18	0.09	0.55	0.79
MgO	2.75	4.94	2.61	2.64	2.46	2.72	2.26	2.56	3.47	MgO	0.05	0.08	0.14	0.19
CaO	6.45	24.7	0.94	0.84	5.21	5.77	3.91	4.42	6.76	CaO	0.26	1.12	4.25	4.97
K_2O	1.59	0.34	2.66	3.68	0.91	1.01	0.86	0.97	1.41	K_2O	2.96	10.21	8.12	6.66
Na_2O	3.41	1.43	0.71	0.84	0.99	1.10	2.5	2.83	3.21	Na_2O	4.32	0.84	2.6	2.77
TiO_2	0.59	0.52	1.57	0.02	0.70	0.78	0.69	0.78	0.73	TiO_2	0.04	0.04	0.13	0.01
MnO	0.13	0.11	0.11	0.00	n.d.	n.d	0.09	0.10	0.14	MnO	0.06	0.03	n.d.	n.d.
Cr_2O_3	<LOD	<LOD	n.d	n.d	n.d.	n.d	<LOD	<LOD	n.d.	CrO	0.03	n.d.	n.d.	n.d.
CuO	n.d	n.d	n.d	n.d	n.d.	n.d	<LOD	<LOD	n.d.	CuO	0.03	n.d.	n.d.	n.d.
P_2O_5	0.27	0.20	0.07	n.d	n.d.	n.d	0.07	0.07	0.10	P_2O_5	n.d.	n.d.	n.d.	n.d.
SO_2	<LOD	0.55	n.d	n.d	n.d.	n.d.	<LOD	<LOD	0.011	S	0.01	n.d.	n.d.	n.d.
Total	98.9	98.6	99.87	98.6	90.3	100	88.4	100	98.5		99.3	100.2	100.04	96.6

For DSDP sites, glass color has not been specified. Note similarity between green glass from this study and Bohor and Betterton (1993), giving both strikingly low analytical totals. Smit et al. (1992b) report pristine, green glass fragments high in Si, Al and K, showing similarities with the high K, Si-rich variety at Beloc. For DSDP 540 and 536 glasses with high Si, Al and K content are reported. Note that in all green glasses, Si, Ca and alkali content seem to vary to a large extent, while Al content is always high, indicating possible admixture of mineral melts $CaAl_2Si_2O_8$, $NaAlSi_3O_8$, $KAlSi_3O_8$ and SiO_2 in various proportions to the bulk homogenized melt sheet.

* Recalculated to 100 wt%.

° Not recalculated.

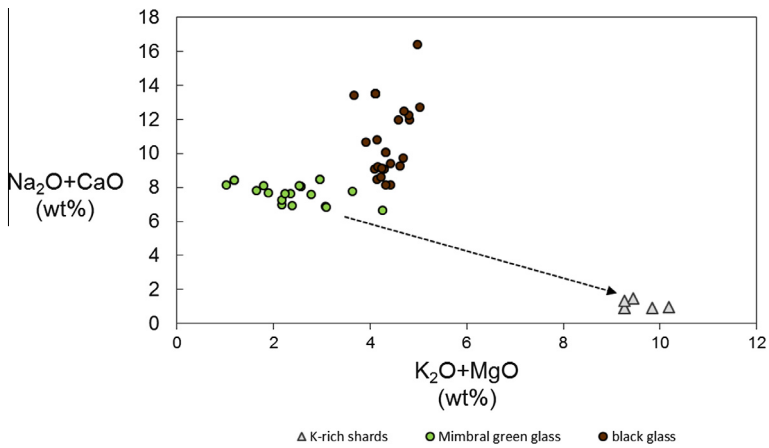

Fig. 26. $Na_2O + CaO$ versus $K_2O + MgO$ diagram for K-rich shards and glasses. Green glasses define a trend with a slope similar to that defined by the K-rich glasses, suggesting a close genetic relationship characterized by Na and Ca exchange with K and Mg. (For interpretation of the references to color in this figure legend, the reader is referred to the web version of this article.)

at the Beloc locality while dominant at Mimbral and at DSDP sites 540 and 536 (Fig. 1).

The observation of green, high SiO_2 glass containing schlieren and cores of low SiO_2 black glass at Mimbral, the presence of (mixed) mineral melts at DSDP 540 and 536 (Alvarez et al., 1992a,b) and mixed CaO-rich and CaO-poor glass at Beloc may indicate heterogeneous and incomplete mixing of the melts ejected from the source crater.

Several studies (Blum et al., 1993; Kettrup et al., 2000; Kettrup and Deutsch, 2003) note that Nd isotopic compositions are highly variable in the impact melt products from the Chicxulub crater. In addition, the compositional heterogeneity of melt particles seems to exceed the compositional diversity of the target rocks because of incomplete mixing between mineral melts and/or rock melts (Tuchscherer, 2008). This is demonstrated by the presence of the (green) high Si, Al, alkali-glass variety (Table 8) showing a compositional range between $CaAl_2Si_2O_8$, $KAlSi_3O_8$, $NaAlSi_3O_8$, SiO_2 end members and the bulk melt sheet composition. Considering the crater's large diameter (~180 km, Hildebrand et al., 1991; Morgan et al., 1997) target heterogeneity across the structure should be expected (Hildebrand et al., 1993). Subsequently, the postulated SE–NW direction of the Chicxulub impactor (Schultz and D'Hondt, 1996) may have caused excavation and melting of deeper target regions down-range, causing a marked variation in the melt distribution in different quadrants from the source crater. The mechanism to produce such heterogeneous melt compositions may result from the unusual lithologies constituting the target beneath Chicxulub: Tuchscherer (2008) emphasizes that the presence of volatiles (H_2O, CO_2 and SO_x) released during shock devolatilization of carbonates, sulfates and water in the target rock beneath Chicxulub would promote rapid fragmentation and dispersion of melt particles, thereby inhibiting homogenization (Kieffer and Simonds, 1980, Hörz et al., 2002). Volatile- enhanced dispersal of generated (heterogeneous) impact melts has also been postulated as a mechanism to produce the large range of tektite compositions ejected from a single crater (see Howard, 2011, for a review). Alternatively, the observed heterogeneity in melt composition may result from liquid immiscibility during cooling. Liquid immiscibility refers to a mechanism into which an originally homogenous melt reaches a temperature where it can no longer remain stable and subsequently unmixes into two liquids of distinctly different composition and density (Roedder, 1978). This may explain why the microtektite glasses from the Chicxulub crater are remarkably homogeneous at the trace element level, but display a large range in major element compositions. Rapid cooling and quenching allowed the originally homogenous melts to exsolve into liquids of contrasting compositions. Diffusion of trace elements was only limited or very slow.

Although green, black and yellow glasses clearly have a common origin as glassy impact melts, it remains unclear why the green variety appears more reduced (Fig. 25, Table 7). Intuitively, more polymerized, high viscosity (high SiO_2) melts are thought to degas less quickly leaving the glasses more oxidized compared to lower SiO_2 melts. Although admixture of carbonate and sulfate target lithologies was proposed as a major oxidizing contributor and can account for the variety in iron oxidation state in the yellow and black glasses (Giuli et al., 2005), other parameters might have contributed to the redox state of iron in impact glasses (e.g., T, P, fO_2, source rock composition). For example, Densem and Turner (1938) have shown that composition plays a major role in determining ferric-ferrous equilibrium in silicate liquids (Kress and Carmichael, 1988). Peraluminous silicate melts have lower $Fe^{3+}/\sum Fe$ compared to peralkaline melts (Dickenson and Hess, 1981). This is the result of the fact that the ferric Fe^{3+} species is present in four-fold coordination and behaves like Al^{3+} (Heide et al., 2001), which is also tetrahedrally coordinated in the silicate structure. Therefore, in peraluminous, Al-rich silicate melts, tetrahedrally coordinated trivalent iron and aluminium will both compete for charge balancing cations. Considering the possibility that green glass from this study represents the hydrated equivalent of the high Si, Al, K-green glasses reported by Smit et al. (1992b) and Alvarez et al. (1992b), the green glasses would have

contained an initial Al_2O_3 content of 20 wt% (Table 8), making competition between Fe^{3+} and Al^{3+} a likely cause for the low iron redox ratio observed in the green glasses from Arroyo El Mimbral.

However, taking into account the hydrated nature of the green high SiO_2 glass type, it must be considered that the redox state could in fact represent a secondary feature, although water is known to be an efficient oxidizer. Noble (1967) noted that hydrated volcanic glasses have significantly lower Fe^{2+}/Fe^{3+} ratios compared to their non-hydrated equivalents. Barkatt et al. (1984) pointed out that iron is leached out of tektites in the highly soluble ferrous (Fe^{2+}) iron form rather than as insoluble ferric iron (Fe^{3+}). In this context, a primary and dominantly ferrous Fe^{2+} state in the green glass variety (Table 7) could explain the low total Fe content (Table 1) in the red glass-interpreted to represent a more advanced stage in the alteration of the green glass, and the development of Fe(-Mg)

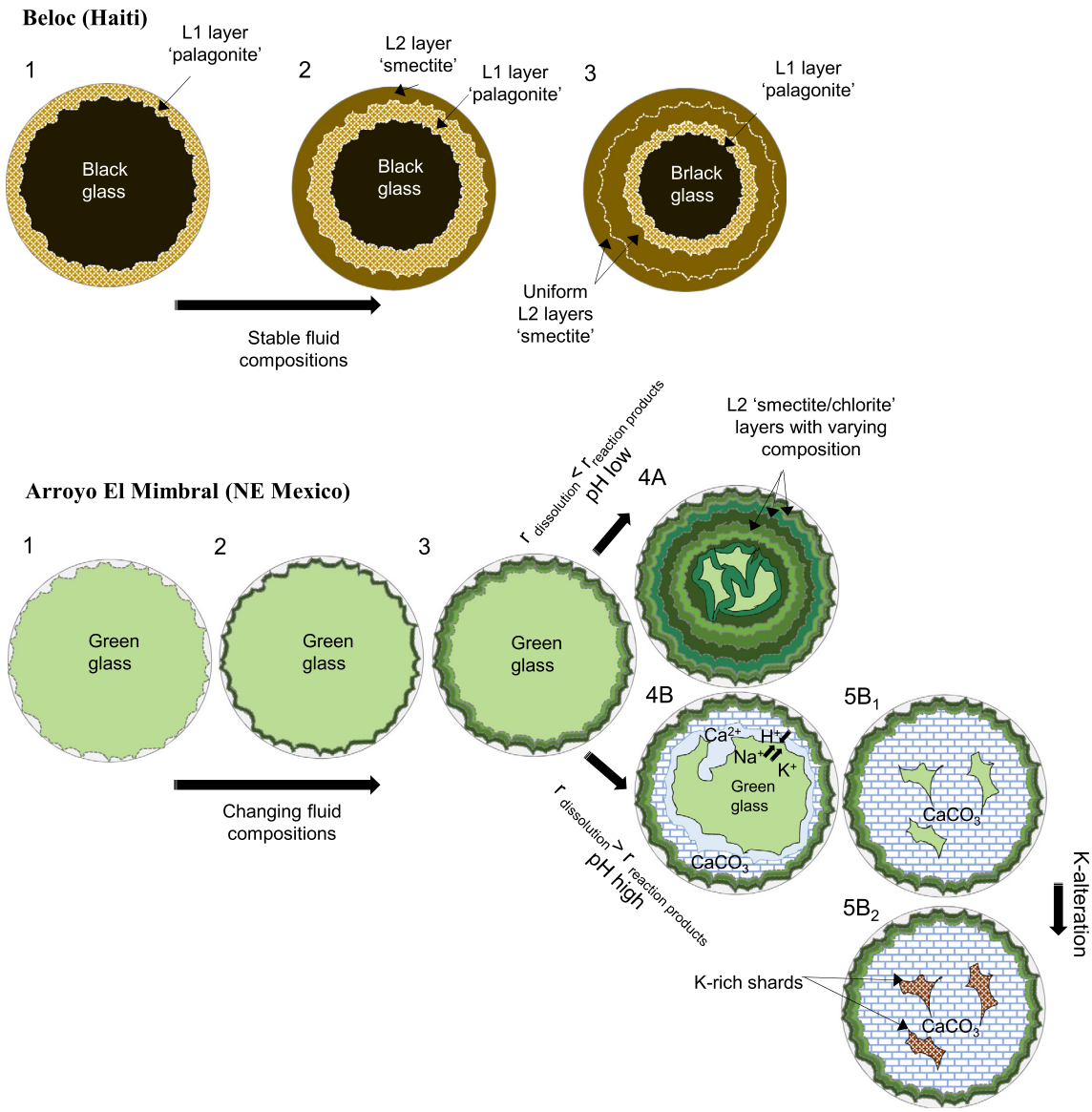

Fig. 27. Simplified sketch showing the postulated alteration mechanism for different glass types. Beloc (Haiti): Black/yellow glass: hydration and formation of a 'palagonite' L1-layer enriched in Al, Fe and Ti. When a sufficient quantity of water is reached, the L1-layer crystallizes into a 'smectite' L2-layer. This process continues as the glass is gradually replaced with hemispherical alteration lamellae that are uniform both at the major and trace element level. Arroyo El Mimbral (NE Mexico): Green glass undergoes several competing reaction processes, dominated by ion exchange, dissolution, water-diffusion and formation of secondary reaction products (hydration–palagonitization). Small, parallel alteration lamellae form when ion-exchange/secondary precipitation is the dominating alteration mechanism, usually under low pH conditions (1–4A). At high pH, dissolution dominates over ion-exchange and the glass will simply dissolve. The formation of secondary calcite rapidly cements the voids and remaining glass pieces in the spherules, often maintaining relict glass pieces in the spherules interior (4B, $4B_1$). If the alteration process is not stalled before complete cementation by calcite, changing fluid compositions and pH as well as restricted water circulation may transform the green hydrated glasses into a K-rich alteration product. (For interpretation of the references to color in this figure legend, the reader is referred to the web version of this article.)

corrosion products at their surface: during initial hydration, the more soluble Fe^{2+} becomes progressively leached from the green glass and accumulates at the glass surface as $Fe(OH)_2$ in aqueous solution. Once saturation is reached, Fe^{2+} may oxidize and recrystallization will occur forming Fe(Mg)-rich alteration products at the surface. Currently, the redox state of different Chicxulub glasses is the focus of more work.

6. CONCLUSION – SUMMARY

This study provides a detailed investigation of different types of microtektite-like glasses linked to the formation of the Chicxulub crater, and their associated alteration products. Both glass composition and fluid properties exert a major control on the type of alteration that has taken place. However, particular textural and geochemical constraints can still be used to deduce the original composition of the glass. This can be particularly useful in areas where pristine glass phases are lacking, providing important clues towards the original composition of the melts ejected from the source crater. A simplified sketch is given in Fig. 27, incorporating all observations and processes that apply to the alteration mechanism of the microtektite spherules from both Beloc and Mimbral locations investigated in this study. A summary of the most important observations is given below:

(1) At Beloc, the alteration process of more mafic low SiO_2 black and yellow glass seems to progress through the formation of palagonite–smectite involving hydration-recrystallization, a well-known mechanism postulated for basaltic glasses. In the first alteration layer, REEs are depleted, but still reflect the CI-normalized pattern of the precursor glass phase. In the second alteration layer, the REEs are almost completely lost to solution and provide no clues towards the original glass composition. Immobile element ratios including HFSEs such as Zr/Hf and Nb/Ta are still representative for the original glass composition.
(2) LA-ICP-MS maps confirm the passive accumulation of insoluble Fe–Ti phases hosting immobile trace elements (e.g., Zr, Hf, Nb, Ta, Ni). Although immobile element ratios still represent the ratio of the precursor, applied spot drilling (55–100 micron) targeting 'nuggets' of residual phases can cause large scatter amongst individual analyses.
(3) For the first time, the green glasses from the Arroyo El Mimbral location have been studied in detail. All green glasses extracted from the deposit appear hydrated. Under low pH conditions, hydration – ion exchange is the dominant alteration process. During hydration, alkalis are leached from the glass network via exchange with H^+ ions from solution. Strontium, Ba, and Cs are taken up from seawater through sorption or minor exchange with Ca or K. Under high pH alkaline conditions, dominating in the calcite-replaced spherules, the glass network will simply dissolve in solution without build-up of insoluble reaction products at the surface. Complex feedback mechanisms between the glass composition and the changing properties of the surrounding fluids may result in the formation of K-rich alteration products with a perlite fabric, a textural characteristic indicative of high silica melts.
(4) The alteration of high SiO_2 (green) glass involves numerous competing reaction processes (Mazer et al., 1991), including molecular water diffusion, ion exchange, surface reaction (etching/dissolution), and secondary mineral precipitation. These reactions are controlled by complex feedback mechanisms between the glass composition and the surrounding fluid. Nonetheless, textural characteristics, such as a perlite fabric, and specific alteration products (such as Fe, Mg-rich and K-rich alteration products) may still provide hints towards the original glass composition.
(5) High SiO_2 glass seems to alter into a high Fe–Mg type product. This is in agreement with observations from Mazer et al. (1992), but strongly contrasts the assumption that chlorite-like alteration products should be related to a mafic precursor, as suggested by Schulte et al. (2003), Kettrup et al. (2000) and Kettrup and Deutsch (2003). Instead, glasses with a more mafic composition, such as the black and yellow glass variety, alter to a smectite-type of alteration product.
(6) Despite the fact that the green glasses form a highly polymerized glass network, these do not appear particularly resistant to aqueous alteration. Although the green glass was initially high in network formers Si and Al, the primary high alkali (K, Na) content compared to low amounts of di-and trivalent cations such as Fe, Mg, Ca makes the green glass highly susceptible to hydration and ion-exchange. In addition, the low Fe^{3+}/Fe^{2+} ratio may have affected glass durability as Fe^{2+} will be more easily solubilized compared to Fe^{3+}.
(7) The dominant presence of green glass at the Mimbral locality as opposed to the low-Si glass variety at Beloc may be attributed to a preservation effect. Alternatively, if the large abundance of green glass fragments is still representative for the original glass distribution, the NW sector in the proximal ejecta field may have been dominated by a more felsic melt composition, putting important constraints on both the cratering dynamics and the target rock compositions.
(8) Microtektite glasses from the Chicxulub crater are remarkably homogenous at the trace element level, but display a large range in major element compositions. This may be the result of liquid immiscibility of an originally more homogenous melt during rapid cooling.
(9) Contrary to black and yellow glasses, green glasses appear significantly reduced. Whether this is a primary feature remains an open question.

ACKNOWLEDGEMENTS

This project was supported by FWO Research Foundation—Flanders (Projects G009113 & GoB8513). We thank Research Foundation-Flanders (FWO) for its support in funding a Ph.D. fellowship to J. Belza and a Postdoctoral Fellowship to S. Goderis. This research has been funded by the Interuniversity Attraction Poles Program Planet Topers initiated by the Belgian Science Policy Office. Oscar Steenhaut and Marc Raes are gratefully acknowledged for technical support with SEM-EDX and FEG-SEM. We would like to thank Christian Koeberl, Axel Wittmann and an anonymous reviewer for corrections and suggestions that have substantially improved the quality of this manuscript.

REFERENCES

Abrajano T. A., Bates J. K. and Mazer J. J. (1989) Aqueous corrosion of natural and nuclear waste glasses: II. Mechanisms of vapor hydration of nuclear waste glasses. *J. Non-Cryst. Solids* **108**, 169–288.

Alvarez W., Grajales N. J. M., Martinez S. R., Romero M. P. R., Ruiz L. E., Guzman R. M. J., Zambrano A. M., Smit J., Swinburne N. H. M. and Margolis S. V. (1992a) The Cretaceous–Tertiary boundary impact-tsunami deposit in NE Mexico. *Geol. Soc. Am. Abstr. Prog.* **24**(7), A331.

Alvarez W., Smit J., Lowrie W., Asaro F., Margolis S. V., Claeys P., Kastner M. and Hildebrand A. R. (1992b) Proximal impact deposits at the Cretaceous–Tertiary boundary in the Gulf of Mexico: A restudy of DSDP Leg 77 Sites 536 and 540. *Geology* **20**, 697–700.

Baert K., Meulebroeck W., Wouters H., Ceglia A., Nys K., Thienpont H. and Terryn H. (2011) Raman spectroscopy as a rapid screening method for ancient plain window glass. *J. Raman Spectrosc.* **42**, 1055–1061.

Baert K., Meulebroeck W., Ceglia A., Wouters H., Cosyns P., Nys K., Thienpont H. and Terryn H. (2012) The potential of Raman spectroscopy in glass studies. In *Conference on Integrated Approaches to the Study of Historical Glass* (IASHG). pp. 8422. (abstr.).

Barkatt A., Boulos M. S., Barkatt A., Sousanpour W., Boroomand M. A., Macedo P. B. and O'Keefe J. A. (1984) The chemical durability of tektites – A laboratory study and correlation with long-term corrosion behavior. *Geochim. Cosmochim. Acta* **48**, 361–371.

Berkgaut V., Singer A. and Stahr K. (1994) Palagonite reconsidered: Paracrystalline illite–smectite from regoliths on basic pyroclastics. *Clays Clay Miner.* **42**, 582–592.

Blum J. D., Chamberlain C. P., Hingston M. P., Koeberl C., Marin L. E., Schuraytz B. C. and Sharpton V. L. (1993) Isotopic comparison of K/T boundary impact glasses with melt rock from the Chicxulub and Manson impact structures. *Nature* **364**, 325–327.

Bohor B. F. and Betterton W. J. (1993) Arroyo el Mimbral, Mexico, K/T unit: Origin as debris flow/turbidite, not a tsunami deposit. In *24th Lunar and Planetary Science Conference*. pp. 143–144. (abstr.).

Bohor B. F. and Glass B. P. (1995) Origin and diagenesis of K/T impact spherules—From Haiti to Wyoming and beyond. *Meteoritics* **30**, 182–198.

Bunker B. C. (1994) Molecular mechanisms for corrosion of silica and silicate glasses. *J. Non-Cryst. Solids* **179**, 300–308.

Claeys P., Alvarez W., Smit J., Hildebrand A. R. and Montanari A. (1993) KT boundary impact glasses from the Gulf of Mexico region. In *24th Lunar and Planetary Science Conference*. pp. 297–298. (abstr.).

Claeys P., Heuschkel S., Lounejeva-Baturina E., Sanchez-Rubio G. and Stöffler D. (2003) The suevite of drill hole Yucatàn 6 in the Chicxulub impact crater. *Meteorit. Planet. Sci.* **38**, 1299–1317.

Colomban P., Etcheverry M.-P., Asquier M., Bounichou M. and Tournié A. (2006) Raman identification of ancient stained glasses and their degree of deterioration. *J. Raman Spectrosc.* **37**, 614–626.

Conde G. D. and Ihinger P. D. (2011) Chemical exchange accompanying obsidian-perlite transition in the natural environment. *Geol. Soc. Am. Abstr. Prog.* **43**(5), 103.

Densem N. E. and Turner W. E. S. (1938) The equilibrium between ferrous and ferric oxides in glasses. *J. Soc. Glass Technol.* **22**, 372–389.

Dickenson M. P. and Hess P. C. (1981) Redox equilibria and the structural role of iron in alumino-silicate melts. *Contrib. Mineral. Petrol.* **78**, 352–357.

Dohmen L., Lenting C., Fonseca R. O. C., Nagel T., Heuser A., Geisler T. and Denkler R. (2013) Pattern formation in silicate glass corrosion zones. *Int. J. Appl. Glass Sci.* **4**, 357–370.

Doremus R. H. (1994) *Glass Science*. John Wiley & Sons, New York, pp. 352.

Dran J. C., Della Mea. G., Paccagnella A., Petit J. C. and Trotignon L. (1988) Aqueous dissolution of alkali silicate glasses: Reappraisal of mechanisms by H and Na depth profiling with high energy ion beams. *Phys. Chem. Glasses* **29**, 249–255.

Dressler B. O. and Reimold W. U. (2001) Terrestrial impact melt rocks and glasses. *Earth-Sci. Rev.* **56**, 205–284.

Fialin M., Wagner C., Métrich N., Humler E., Galoisy L. and Bézos A. (2001) Fe3+/$\sum$Fe vs. FeLα peak energy for minerals and glasses: Recent advances with the electron microprobe. *Am. Mineral.* **86**, 456–465.

Fisher R. V. and Schmincke H.-U. (1984) *Pyroclastic Rocks*. Springer-Verlag, New York, 472.

French B. M. (1998) *Traces of catastrophe: A handbook of shock-metamorphic effects in terrestrial meteorite impact structures*. Lunar and Planetary Institute, Houston, 120.

Friedman I. and Long W. (1976) Hydration rate of obsidian. *Science* **191**, 347–352.

Friedman I. and Smith R. L. (1958) The deuterium content of water in some volcanic glasses. *Geochim. Cosmochim. Acta* **15**(218–220), 221–228.

Friedman I., Smith R. L. and Long W. D. (1966) Hydration of natural glass and formation of perlite. *Bull. Geol. Soc. Am.* **77**, 323–328.

Gislason S. R. and Eugster H. P. (1987) Meteoric water-basalt interaction I: A laboratory study. *Geochim. Cosmochim. Acta* **51**, 2827–2840.

Gislason S. R., Veblen D. R. and Livi K. J. T. (1993) Experimental meteoric water-basalt interactions: Characterisation and interpretation of alteration products. *Geochim. Cosmochim. Acta* **57**, 1459–1471.

Giuli G., Eeckhout S. G., Paris E., Koeberl C. and Pratesi G. (2005) Iron oxidation state in impact glass from the K/T boundary at Beloc, Haiti, by high-resolution XANES spectroscopy. *Meteorit. Planet. Sci.* **40**, 1575–1580.

Giuli G., Eeckhout S. G., Koeberl C., Pratesi G. and Paris E. (2008) Yellow impact glass from the K/T boundary at Beloc (Haiti): XANES determination of the Fe oxidation state and implications for formation conditions. *Meteorit. Planet. Sci.* **43**, 981–986.

Glass B. P., Burns C. A., Lerner D. H. and Sanfilippo A. (1984) North American tektites and microtektites from Barbados, West Indies. *Meteoritics* **19**, 228–229.

Glass B. P. and Simonson B. M. (2012) Distal impact ejecta layers: Spherules and more. *Elements* **8**(1), 43–48.

Goderis S., Hertogen J., Vanhaecke F. and Claeys P. (2010) Siderophile elements from the Eyreville drill cores of the Chesapeake Bay impact structure do not constrain the nature of the projectile. In *Large Meteorite Impacts and Planetary Evolution IV* (eds. R. L. Gibson and W. U. Reimold). Geological Society of America Special Paper, Boulder, pp. 395–409.

Haskin L. A., Wildeman T. R., Frey F. A., Collins K. A., Keedy C. R. and Haskin M. A. (1966) Rare earths in sediments. *J. Geophys. Res.* **71**, 6091–6105.

Heide K. and Heide G. (2011) Vitreous state in nature – Origin and properties. *Chem. Erde Geochem.* **71**, 305–335.

Heide K., Heide G. and Kloess G. (2001) Glass chemistry of tektites. *Planet. Space Sci.* **49**, 839–844.

Hildebrand A. R., Gregoire D. C., Attrep M. J., Claeys P., Thompson C. M. and Boynton W. V. (1993) Trace-element composition of Chicxulub crater melt rock, K/T tektites and Yucatan basement. In *24th Lunar and Planetary Science Conference*. pp. 657–658. (abstr.).

Hildebrand A. R., Penfield G. T., Kring D. A., Pilkington M., Camargo Z. A., Jacobsen S. B. and Boynton W. V. (1991) Chicxulub Crater: A possible Cretaceous/Tertiary boundary impact crater on the Yucatán Peninsula, Mexico. *Geology* **19**, 867–871.

Hörz F. (1982) Ejecta of the Ries Crater, Germany. In *Geological Implications of Impacts of Large Asteroids and Comets on Earth* (eds. L. T. Silver and P. H. Schultz). Geological Society of America special Paper, Boulder, pp. 39–55.

Hörz F., Mittlefehldt D. W., See T. H. and Galindo C. (2002) Petrographic studies of the impact melts from Meteor Crater, Arizona. *USA. Meteorit. Planet. Sci.* **37**, 501–531.

Howard K. T. (2011) Volatile enhanced dispersal of high velocity impact melts and the origin of tektites. *P. Geologist. Assoc.* **122**(3), 363–382.

Hunt J. B. and Hill P. G. (1993) Tephra geochemistry: A discussion of some persistent analytical problems. *Holocene* **3**, 271–278.

Izett G. A. (1991a) K–T boundary tektites from near Beloc, Haiti. In *Abstracts of the Lunar and Planetary Science Conference*, vol. 22. p. 625.

Izett G. A. (1991b) Tektites in Cretaceous–Tertiary boundary rocks on Haiti and their bearing on the Alvarez impact extinction hypothesis. *J. Geophys. Res.* **96**(20), 879-820, 905.

Izett G. A., Maurrasse F. J.-M. R., Lichte F. E., Meeker G. P. and Bates R. (1990) Tektites in Cretaceous–Tertiary boundary rocks on Haiti. *U.S. Geol. Surv. Open-File Rep.* **90–635**, 1–31.

Izett G. A., Dalrymple G. B., Snee L. W. and Pringle M. S. (1991) $^{40}Ar/^{39}Ar$ age (66–64 Ma) of K–T boundary tektites. In *Abstracts of the Lunar and Planetary Science Conference*, vol. 22. p. 627.

Izmer A., Goderis S., Simonson B. M., McDonald I., Hassler S. W., Claeys P. and Vanhaecke F. (2013) Application of laser ablation-ICP-mass spectrometry for 2-dimensional mapping of element distributions in a Late Archean impact spherule layer. *J. Anal. Atom. Spectrom.* **28**, 1031–1038.

Jercinovic M. J., Keil K., Smith M. R. and Schmitt R. A. (1990) Alteration of basaltic glasses from north-central British Columbia, Canada. *Geochim. Cosmochim. Acta* **54**, 2679–2696.

Jezek P. A. and Noble D. C. (1978) Natural hydration and ion exchange of obsidian: An electron microprobe study. *Am. Mineral.* **63**, 266–273.

Keller W. D., Reynolds R. C. and Atsuyuki I. (1986) Morphology of clay minerals in the smectite-to-illite conversion series by scanning electron microscopy. *Clays Clay Miner.* **34**, 187–197.

Kettrup B. and Deutsch A. (2003) Geochemical variability of the Yucatàn basement: Constraints from crystalline clasts in Chicxulub impactites. *Meteorit. Planet. Sci.* **38**, 1079–1092.

Kettrup B., Deutsch A., Ostermann M. and Agrinier P. (2000) Chicxulub impactites: Geochemical clues to the precursor rocks. *Meteorit. Planet. Sci.* **35**, 1229–1238.

Kieffer S. W. and Simonds C. H. (1980) The role of volatiles and lithology in the impact cratering process. *Rev. Geophys. Space Phys.* **18**(1), 143–181.

Koeberl C. (1986) Trace element correlations as clues to the origin of tektites and impactites. *Chem. Erde* **45**, 1–21.

Koeberl C. (1993) Chicxulub Crater, Yucatan – Tektites, impact glasses, and the geochemistry of target rocks and breccias. *Geology* **21**, 211–214.

Koeberl C. h. and Sigurdsson H. a. (1992) Geochemistry of impact glasses from the K/T boundary in Haiti: Relation to smectites and a new type of glass. *Geochim. Cosmochim. Acta* **56**, 2113–2129.

Kress V. C. and Carmichael I. S. E. (1988) Stoichiometry of the iron oxidation reaction in silicate melts. *Am. Mineral.* **73**, 1267–1274.

Kring D. A. (1995) The dimensions of the Chicxulub impact crater and impact melt sheet. *J. Geophys. Res.* **100**, 16979–16986.

Kring D. A. and Boynton W. V. (1991) Altered spherules of impact melt and associated relic glass from the K/T boundary sediments in Haiti. *Geochim. Cosmochim. Acta* **55**, 1737–1742.

Kring D. A. and Boynton W. V. (1992) Petrogenesis of an augite-bearing melt rock in the Chicxulub structure and its relationship to K/T impact spherules in Haiti. *Nature* **358**, 141–144.

Le Losq C., Neuville D. R., Moretti R. and Roux J. (2012) Determination of water content in silicate glasses using Raman spectrometry: Implications for the study of explosive volcanism. *Am. Mineral.* **97**, 779–790.

Lodders K., Palme H. and Gail H. P. (2009) Abundances of the elements in the solar system. In *Landolt- Bornstein, New Series* (ed. J. E. Trumper). Springer-Verlag, Berlin, Heidelberg, New York, pp. 560–630.

López-Ramos E. (1975) Geological summary of the Yucatán Peninsula. In *The Ocean Basins and Margins, v. 3: The Gulf of Mexico and the Caribbean* (eds. A. E. M. Nairn and F. G. Stehli). Plenum, New York. pp. 257–282.

Maurasse F. J.- M. R., Pierre-Louis F. and Rigaud J. J. -G. (1979) Upper Cretaceous to Lower Paleocene pelagic calcareous deposits in the Southern Peninsula of Haiti: Their bearing on the problem of the Cretaceous–Tertiary boundary. In *Fourth Latin American Geological Congress*. pp. 328–338. (abstr.).

Mazer J. J., Stevenson C. M., Ebert W. L. and Bates J. K. (1991) The experimental hydration of obsidian as a function of relative humidity and temperature. *Am. Antiquity* **56**, 504–513.

Mazer J. J., Bates J. K., Bradley J. P., Bradley C. R. and Stevenson C. M. (1992) Alteration of Tektite to form weathering products. *Nature* **357**, 573–576.

Meisinger A. C. (1980) Perlite, Mineral Facts and Problems, Bulletin 671, US Bureau of mines. pp. 1–12.

Melosh H. J. (1989) *Impact Cratering: A Geologic Process*. Oxford University Press, New York, 245.

Morgan J., Warner M., Brittan J., Buffler R., Camargo A., Christeson G., Denton P., Hildebrand A., Hobbs R., Macintyre H., Mackenzie G., Maguire P., Marin L., Nakamura Y., Pilkington M., Sharpton V., Snyder D., Suarez G. and Trejo A. (1997) Size and morphology of the Chicxulub impact crater. *Nature* **390**, 472–476.

Morgenstein M. and Riley T. J. (1974) Hydration-rind dating of basaltic glass: A new method for archaeological chronologies. *Asian Perspect.* **17**, 145–159.

Noble D. D. (1967) Sodium, potassium and ferrous iron contents of some secondarily hydrated natural silicic glasses. *Am. Mineral.* **52**, 280–286.

Noh J. H. and Boles J. R. (1989) Diagenetic alteration of perlite in the Guryongpo area, Republic of Korea. *Clays Clay Miner.* **37**, 47–58.

Otha A. and Kwave I. (2001) REE(III) adsorption onto Mn dioxide (δ-MnO_2) and Fe oxyhydroxide: Ce(III) oxidation by δ-MnO_2. *Geochim. Cosmochim. Acta* **65**, 695–703.

Petit J. C., Mea G. D., Dran J. C., Magonthier M. C., Mando P. A. and Paccagnella A. (1990) Hydrated-layer formation during dissolution of complex silicate glasses and minerals. *Geochim. Cosmochim. Acta* **54**, 1941–1955.

Pierazzo E. and Melosh H. J. (1999) Hydrocode modeling of Chicxulub as an oblique impact event. *Earth Planet. Sci. Lett.*, 163–176

Pierazzo E., Vickery A. M. and Melosh H. J. (1997) A reevaluation of impact melt production. *Icarus* **127**, 408–423.

Pierazzo E., Kring D. A. and Melosh H. J. (1998) Hydrocode simulation of the Chicxulub impact event and the production of climatically active gases. *J. Geophys. Res.-Planet.* **103**, 28607–28625.

Premo W. R. and Izett G. A. (1991) Nd–Sr isotopic signature of tektites form the K/T boundary in Haiti. In *Abstracts of the Lunar and Planetary Science Conference*, vol. 22. pp. 1091–1092.

Premo W. R. and Izett G. A. (1992) Isotopic signatures of black tektites from the K–T boundary on Haiti: Implications for the age and type of source material. *Meteoritics* **27**, 413–423.

Premo W. R., Izett G. A. and Meeker G. P. (1995) Major-element and isotopic compositions of relic tektites and glass-like shards from the K–T boundary bed at El Mimbral, Mexico. In *Abstracts of the Lunar and Planetary Science Conference*, vol. 26. p. 1139.

Ridley W. I. (2012) Petrology of associated igneous rocks in volcanogenic massive sulfide occurence model. U.S Geological Survey Investigations Scientific Report 2010-5070. p. 32.

Robinet L., Coupry C., Eremin K. and Hall C. (2006) Raman investigation of the structural changes during alteration of historic glasses by organic pollutants. *J. Raman Spectrosc.* **37**, 1278–1286.

Robinet L., Bouquillon A. and Hartwig J. (2008) Correlations between Raman parameters and elemental composition in lead and lead alkali silicate glasses. *J. Raman Spectrosc.* **39**, 618–626.

Roedder E. (1978) Silicate liquid immiscibility in magmas and in the system K_2O–FeO–Al_2O_3–SiO_2: An example of serendipity. *Geochim. Cosmochim. Acta* **42**, 1597–1617.

Rothwell R. G. (1989) *Minerals and Mineraloids in Marine Sediments: An Optical Identification Guide*. Elsevier Applied Science, London., 279 pp.

Scholze H. and Mulfinger H. O. (1959) Der Einbau des Wassers in Gläsern V. Die Diffusion des Wassers in Gläsern bei hohen Temperaturen. *Glastechn. Ber.* **32**, 381–386.

Schulte P., Stinnesbeck W., Stüben D., Kramar U., Berner Z., Keller G. and Adatte T. (2003) Fe-rich and K-rich mafic spherules from slumped and channelized Chicxulub ejecta deposits in the northern La Sierrita area, NE Mexico. *Int. J. Earth Sci.* **92**, 114–142.

Schultz P. H. and D'hondt S. (1996) Cretaceous–Tertiary (Chicxulub) impact angle and its consequences. *Geology* **24**, 963–967.

Schuraytz B. C., Sharpton V. L. and Marin L. E. (1994) Petrology of impact-melt rocks at the Chicxulub multiring basin, Yucatán, Mexico. *Geology* **22**, 868–872.

Shaw H. F. and Wasserburg G. J. (1982) Age and provenance of the target materials for tektites and possible impactites as inferred from Sm–Nd and Rb–Sr systematics. *Earth Planet. Sci. Lett.* **60**, 155–177.

Sigurdsson H., Bonte P., Turpin L., Chaussidon M., Metrich N., Steinberg M., Pradel P. and D'Hondt S. (1991a) Geochemical constraints on source region of Cretaceous/Tertiary impact glasses. *Nature* **353**, 839–842.

Sigurdsson H., D'Hondt S., Arthur M. A., Bralower T. J., Zachos J. C., Van Fossen M. and Channell J. E. T. (1991b) Glass from the Cretaceous/Tertiary boundary in Haiti. *Nature* **349**, 482–487.

Smit J. (1999) The global stratigraphy of the Cretaceous–Tertiary boundary impact ejecta. *Annu. Rev. Earth Planet. Sci. Lett.* **27**, 75–113.

Smit J. and Alvarez W. (1991) Is the "Mid-Cretaceous Unconformity" in the Gulf of Mexico a Cretaceous–Tertiary boundary impact-wave erosion surface? In *Abstracts of the Lunar and Planetary Science Conference*, vol. 22. pp. 1275–1276.

Smit J., Grajales M., Alvarez W., Swinburne N. H. M. and Montanari A. (1992a) Sedimentology and biostratigraphy of Cretaceous–Tertiary impact-tsunami wave deposits in NE Mexico and Texas. *Geol. Soc. Am. Abstr. Prog.* **24**(7), A355.

Smit J., Montanari A., Swinburne N. H. M., Alvarez W., Hildebrand A. R., Margolis S. V., Claeys P., Lowrie W. and Asaro F. (1992b) Tektite-bearing, deep-water clastic unit at the Cretaceous–Tertiary boundary in Northeastern Mexico. *Geology* **20**, 99–103.

Smit J., Roep T. B., Alvarez W., Montanari A., Claeys P., Grajales Nishimura J. M. and Bermudez J. (1996) Coarse-grained, clastic sandstone complex at the KT boundary around the Gulf of Mexico: Deposition by tsunami waves induced by the Chicxulub impact. In *The Cretaceous-Tertiary Boundary Event and other Catastrophes in Earth History* (eds. G. Ryder, D. Fastovsky and S. Gartner). Geological Society of America Special Paper, Boulder, Colorado, pp. 151–182.

Staudigel H. and Hart S. R. (1983) Alteration of basaltic glass: Mechanisms and significance for the oceanic crust-seawater budget *Geochim. Cosmochim. Acta* **47**, 337–350.

Steefel C. I. and Lasaga A. C. (1994) A coupled model for transport of multiple chemical species and kinetic precipitation/dissolution reactions with application to reactive flow in single phase hydrothermal systems. *Am. J. Sci.* **294**, 529–592.

Stroncik N. and Schmincke H.-U. (2002) Palagonite – A review. *Int. J. Earth Sci.* **91**, 680–697.

Stumm W. and Morgan J. J. (1996) *Aquatic Chemistry: Chemical Equilibria and Rates in Natural Waters*. Wiley, New York, p. 1022.

Swisher C. C., Grajales-Nishimura J. M., Montanari A., Margolis S. V., Claeys P., Alvarez W., Renne P., Cedillo-Pardo E., Maurrasse F. J.-M. R., Curtis G. H., Smit J. and McWilliams M. O. (1992) Coeval $^{40}Ar/^{39}Ar$ ages of 65.0 million years ago from Chicxulub crater melt rock and Cretaceous–Tertiary boundary tektites. *Science* **257**, 954–958.

Taylor S. R. and McLennan S. M. (1995) The geochemical evolution of the continental crust. *Rev. Geophys.* **33**, 241–265.

Tuchscherer M. G. (2008) The petrology and geochemistry of the impactite sequence and selected target rocks from the Yaxcopoil-1 borehole, Chicxulub Impact Structure, Yucatan Peninsula, Mexico, Ph. D. thesis. University of Witwatersrand, Johannesburg, South Africa. p. 376.

Ulrich T., Kamber B. S., Jugo P. J. and Tinkham D. K. (2009) Imaging element-distribution patterns in minerals by laser ablation-inductively coupled plasma-mass spectrometry. *Can. Mineral.* **47**, 1001–1012.

Urrutia-Fucugauchi J., Morgan J., Stoeffler D. and Claeys P. (2004) The Chicxulub scientific drilling project (CSDP). *Meteorit. Planet. Sci.* **39**, 787–790.

Utton C. A., Hand R. J., Bingham P. A., Hyatt N. C., Swanton S. W. and Williams S. J. (2013) Dissolution of vitrified wastes in a high-pH calcium-rich solution. *J. Nucl. Mater.* **435**, 112–122.

Ward W. C., Keller G., Stinnesbeck W. and Adatte T. (1995) Yucatan subsurface stratigraphy: Implications and constraints for the Chicxulub impact. *Geology* **23**, 873–876.

Warren P. H., Claeys P. and Cedillo-Pardo E. (1996) Mega-impact melt petrology (Chicxulub, Sudbury, and the Moon): Effects of scale and other factors on potential for fractional crystallization and development of cumulates. In *The Cretaceous–Tertiary Boundary Event and other Catastrophes in Earth History* (eds. G. Ryder, D. Fastovsky and S. Gartner). Geological Society of America Special Paper, Boulder, Colorado, pp. 105–124.

Wünnemann K., Collins G. S. and Osinski G. R. (2008) Numerical modelling of impact melt production in porous rocks. *Earth Planet. Sci. Lett.* **269**, 530–539.

Zhong S. and Mucci A. (1995) Partitioning of rare earth elements (REEs) between calcite and seawater solutions at 25 °C and 1 atm, and high dissolved REE concentrations. *Geochim. Cosmochim. Acta* **59**, 443–453.

Associate editor: Christian Koeberl